The Astrophysical Journal, 695:1163–1182, 2009 April 20 doi:10.1088/0004-637X/695/2/1163

SPECTROSCOPIC OBSERVATIONS OF LYMAN BREAK GALAXIES AT REDSHIFTS ∼4, 5, AND 6 IN THE GOODS-SOUTH FIELD*

E. Vanzella[1], M. Giavalisco[2], M. Dickinson[3], S. Cristiani[1,4], M. Nonino[1], H. Kuntschner[5], P. Popesso[6], P. Rosati[6], A. Renzini[7], D. Stern[8], C. Cesarsky[6], H. C. Ferguson[9], R. A. E. Fosbury[5], and the GOODS Team
[1] INAF-Osservatorio Astronomico di Trieste, via G. B. Tiepolo 11, 40131 Trieste, Italy
[2] Astronomy Department, University of Massachusetts, Amherst, MA 01003, USA
[3] NOAO, P.O. Box 26732, Tucson, AZ 85726, USA
[4] INFN, National Institute of Nuclear Physics, via Valerio 2, I-34127 Trieste, Italy
[5] ST-EFC, Karl Schwarzschild Strasse 2, 85748 Garching, Germany
[6] ESO, Karl Schwarzschild Strasse 2, 85748 Garching, Germany
[7] INAF-Osservatorio Astronomico di Padova, Vicolo dell'Osservatorio 5, 35122 Padova, Italy
[8] JPL, California Institute of Technology, Mail Stop 169-527, Pasadena, CA 91109, USA
[9] STScI, 3700 San Martin Dr., Baltimore, MD 21218, USA
Received 2008 October 17; accepted 2009 January 29; published 2009 April 6

ABSTRACT

We report on observations of Lyman break galaxies (LBGs) selected from the Great Observatories Origins Deep Survey at mean redshifts $z \sim 4$, 5, and 6 (B_{435}-, V_{606}-, and i_{775}-band dropouts, respectively), obtained with the red-sensitive FORS2 spectrograph at the ESO VLT. This program has yielded spectroscopic identifications for 114 galaxies (∼60% of the targeted sample), of which 51 are at $z \sim 4$, 31 at $z \sim 5$, and 32 at $z \sim 6$. We demonstrate that the adopted selection criteria are effective, identifying galaxies at the expected redshift with minimal foreground contamination. Of the 10% interlopers, 83% turn out to be Galactic stars. Once selection effects are properly accounted for, the rest-frame ultraviolet (UV) spectra of the higher redshift LBGs appear to be similar to their counterparts at $z \sim 3$. As at $z \sim 3$, LBGs at $z \sim 4$ and $z \sim 5$ are observed with Lyα both in emission and in absorption; when in absorption, strong interstellar lines are also observed in the spectra. The stacked spectra of Lyα absorbers and emitters also show that the former have redder UV spectra and stronger but narrower interstellar lines, a fact also observed at $z \sim 2$ and 3. At $z \sim 6$, sensitivity issues bias our sample toward galaxies with Lyα in emission; nevertheless, these spectra appear to be similar to their lower redshift counterparts. As in other studies at similar redshifts, we find clear evidence that brighter LBGs tend to have weaker Lyα emission lines. At fixed rest-frame UV luminosity, the equivalent width of the Lyα emission line is larger at higher redshifts. At all redshifts where the measurements can be reliably made, the redshift of the Lyα emission line turns out to be larger than that of the interstellar absorption lines (ISLs), with a median velocity difference $\Delta V \sim 400$ km s^{-1} at $z \sim 4$ and 5, consistent with results at lower redshifts. This shows that powerful, large-scale winds are common at high redshift. In general, there is no strong correlation between the morphology of the UV light and the spectroscopic properties. However, galaxies with deep ISLs and strong Lyα absorption appear to be more diffuse than galaxies with Lyα in emission.

Key words: cosmology: observations – galaxies: distances and redshifts – galaxies: evolution – galaxies: formation

Online-only material: color figures

1. INTRODUCTION

The study of galaxies at high redshift is crucial for understanding the formation of the Hubble sequence, the growth of visible structures in the universe, and the processes leading to the re-ionization of the intergalactic hydrogen at the end of the Dark Ages. In the past decade, the empirical investigation of galaxies at high redshifts (i.e., $z > 1.5$) has made rapid progress; thanks to advances in telescopes and instrumentation and to the development of optimized selection techniques based on the observed colors of galaxies through either broad or narrow passbands. Color-selection criteria, which are designed to target galaxies with a range of spectral energy distributions (SEDs) within a targeted redshift window, are generally very efficient and allow one to build large samples with reasonably well-controlled systematics (e.g., Steidel et al. 1999; Daddi et al. 2004; van Dokkum et al. 2003; Taniguchi et al. 2005), suitable for a broad range of studies, both statistical in character or based on the properties of the individual sources.

Among the various types of galaxies at high redshifts identified by color selection, the Lyman break galaxies (LBGs; e.g., Guhathakurta et al. 1990; Steidel et al. 2003; Giavalisco et al. 2004b; for a review, see Giavalisco 2002) are the best studied and their samples are the largest both from a statistical point of view, and in terms of the cosmic time covered (reaching back to less than one billion years after the big bang). The reason is mostly practical: since these galaxies are selected on the basis of luminous rest-frame ultraviolet (UV) emission, which at redshifts $2.5 \lesssim z \lesssim 6$ is redshifted into the optical and near-infrared (near-IR) windows, the observations are among the easiest to carry out, taking advantage of very sensitive instrumentation with large areal coverage.

LBGs at redshift $z \sim 3$ have been intensively studied with both very large (Steidel et al. 2003) and deep samples (Papovich

* Based on observations made at the European Southern Observatory Very Large Telescope, Paranal, Chile (ESO programme 170.A-0788 The Great Observatories Origins Deep Survey: ESO Public Observations of the *SST* Legacy/*HST* Treasury/Chandra Deep Field-South). Also based on observations obtained with the NASA/ESA *Hubble Space Telescope* obtained at the Space Telescope Science Institute, which is operated by the Association of Universities for Research in Astronomy, Inc. (AURA) under NASA contract NAS 5-26555.

et al. 2001), including high-quality spectra for more than a thousand galaxies. Current surveys at $z \sim 3$ provide the largest data set to study the properties of galaxies during a relatively early phase of galaxy evolution ($z \sim 3$ corresponds to when the universe was ∼20% of its current age), at least for one spectral type, namely star-forming galaxies with moderate dust obscuration. A number of follow-up studies have been carried out following the discovery of these galaxies (Steidel et al. 1996a, 1996b), including studies of their morphology and size (Giavalisco et al. 1996; Papovich et al. 2003; Ravindranath et al. 2006; Law et al. 2007; Lotz et al. 2006; Ferguson et al. 2004), their ages and stellar masses (Papovich et al. 2001; Shapley et al. 2001; Dickinson et al. 2003a), their chemical evolution (Pettini et al. 2000; Shapley et al. 2003), and of their clustering properties (Giavalisco et al. 1998; Adelberger et al. 1998, 2003; Giavalisco & Dickinson 2001).

At higher redshifts, LBGs appear fainter, the observations require higher sensitivity and the samples are still relatively small. As a consequence, the properties of the most-distant LBGs are less well characterized. Initial studies of the spectral properties and luminosity function have been carried out at $z \sim 4$ (Steidel et al. 1999) and $z \sim 5$ (Madau et al. 1998) based on fairly small samples. More recently, larger samples at $z > 4$ have been gathered, from both ground- and space-based observatories (Shimasaku et al. 2005; Iwata et al. 2003; Giavalisco et al. 2004b; Dickinson et al. 2004; Bunker et al. 2004; Bouwens et al. 2006, 2007); these samples, however, are exclusively photometric ones, with small numbers of spectroscopic identifications. Such studies have investigated a wide spectrum of statistical properties of LBGs at $z > 4$ and up to $z \sim 7$, such as spatial clustering, morphology, UV luminosity function, stellar mass, and properties of the Lyα line (see, for example, Hamana et al. 2006; Lee et al. 2006; Ravindranath et al. 2006; Lotz et al. 2006; Giavalisco et al. 2004b; Ferguson et al. 2004; Ouchi et al. 2005; Bouwens et al. 2007; Ando et al. 2006, 2007; Yan et al. 2006). However, these results are based on the assumption that the spectral properties of LBGs at $z \gtrsim 4$ are the same as at $z \sim 3$. It is reasonable to expect that the higher redshift samples should bear a similarity to those at $z \sim 3$, since LBG color selection at all redshifts is tuned to select galaxies with a similar rest-frame UV SED. However, without spectroscopic information, it is impossible to know if evolutionary effects are introducing systematic biases in the observed statistics. For example, if the distribution of surface brightness, UV SED, or Lyα emission line properties evolve with redshift, this will affect the redshift distribution and the completeness of the samples, which in turn will bias derived properties such as the LBG spatial clustering, luminosity function, and the evolution of these quantities.[10]

In this paper, we present results from a program of spectroscopic follow up of LBGs at redshift $z > 4$ selected from optical images obtained with the Advanced Camera for Surveys (ACS; Ford et al. 1998) on board the *Hubble Space Telescope* (*HST*) in the four passbands, B_{435}, V_{606}, i_{775}, and z_{850}, as part of the Great Observatories Origins Deep Survey (GOODS; for an overview of the GOODS project, see Renzini et al. 2003; Dickinson et al. 2003b; Giavalisco et al. 2004a). The spectra have been obtained at the ESO VLT with the FORS2 spectrograph. The data from this program, specifically all the spectra of galaxies in the redshift range 0.5–6.3, have already been released and described in previous papers (Vanzella et al. 2005, 2006, 2008). Here we focus on a sample of LBGs, which has yielded 114 spectroscopic identifications in the redshift interval 3.1–6.3. Re-analyzing the whole LBG sample, we introduce very few differences (mainly in the quality redshift) to respect the previous global release (Vanzella et al. 2008), improvements that have been marked in the reported list of the present work. Currently, it represents one of the largest and most homogeneously selected spectroscopic samples in this redshift range.

Throughout this paper, magnitudes are in the AB scale (Oke 1974), and the world model, when needed, is a flat universe with density parameters $\Omega_m = 0.27$, $\Omega_\Lambda = 0.73$, and Hubble constant $H_0 = 73$ km s^{-1} Mpc^{-1}.

2. DATA AND SAMPLE SELECTION

2.1. ACS Images and Source Catalogs

We have selected samples of LBGs at mean redshift $z \sim 4$, 5, and 6 (in the following referred to as B_{435}-, V_{606}-, and i_{775}-band dropouts, respectively) from the latest version (v2.0) of the GOODS images, obtained with the ACS on *HST*. The v2.0 mosaics are nearly identical in shape and size to the v1.0 ones. They cover the two GOODS fields, the northern one encompassing the Hubble Deep Field-North (HDF-N) and the southern one located at the center of the Chandra Deep Field-South (CDF-S). Each subtend an area of approximately 10×17 arcmin on the sky, for a total areal coverage of about 0.1 deg^2. As with v1.0, the v2.0 images consist of two sets of mosaics observed in the B_{435}, V_{606}, i_{775}, and z_{850} filters. The depth of the V_{606}, i_{775}, and z_{850} mosaics, however, has been increased over version v1.0 by including additional observations taken during the continuation of the original GOODS Survey for high-redshift Type Ia supernovae (Riess et al. 2004, 2005). Since these additional data were obtained using the same observational strategy as the original ACS program (e.g., the same Phase-II files were used to carry out the observations), integrating them into the existing mosaics has been straightforward and has resulted in doubling the original exposure time in the z_{850} band as well as a more modest depth increase in the other bands.[11]

2.2. Photometric Samples of Lyman Break Galaxies

We have selected samples of LBGs using color criteria very similar to those presented by Giavalisco et al. (2004b; hereafter G04b), with some minor modifications applied to the definition of B_{435}-band dropouts to explore the redshift distribution of galaxies near the border of that color–color selection window. The exact locations of such windows balance the competing desires of completeness and reliability. Windows are designed to include as complete a sample of target galaxies as possible given the dispersion of observed colors—due to both observational scatter and the intrinsic dispersion in galaxy UV SEDs (e.g., related to varying dust content, ages, metallicities, Lyα equivalent widths, etc.). On the other hand, windows are designed to avoid significant numbers of galaxies at redshifts outside (usually lower than) the targeted one.

[10] Note that a simple analysis of the *observed* colors or sizes is not sufficient to establish the presence of evolutionary effects since it is not possible to separately measure the distribution functions of color, size, and luminosity. See discussion in Reddy et al. (2008).

[11] The v2.0 exposure times in the B_{435}, V_{606}, i_{775}, and z_{850} bands are 7200, 5450, 7028, and 18,232 s, respectively. Details of the ACS observations, as well as major features of the GOODS project, can be found in Giavalisco et al. (2004a); additional information about the latest v2.0 release of the GOODS ACS images and source catalogs can be found at Web site www.stsci.edu/science/goods/ and will be described in detail in an upcoming paper (M. Giavalisco et al. 2009, in preparation).

In the present work, B_{435}-band dropouts are defined as objects that satisfy the color equations

$$(B_{450} - V_{606}) \geqslant 1.1 + (V_{606} - z_{850}) \wedge (B_{450} - V_{606}) \geqslant 1.1 \wedge (V_{606} - z_{850}) \leqslant 1.6, \quad (1.1)$$

where $\wedge$ and $\vee$ are the logical AND and OR operators. These criteria extend the selection of candidates to slightly bluer (B_{435}–V_{606}) and redder (V_{606}–z_{850}) colors than those in G04b. As can be seen in Figure 1, which shows the selection windows corresponding to both sets of color equations, the sample selected with the new criteria (solid line) fully includes the one selected with the G04b criteria (dashed line). We have decided to use these more general criteria to define the sample of B_{435}-band dropouts, which is the largest among the three LBG samples targeted for the spectroscopic observations, to explore both changes in the low end of the targeted redshift range and contamination rates from low-redshift interlopers.

The definitions of the color equations of V_{606}- and i_{775}-band dropouts are unchanged from those used in G04b and Dickinson et al. (2004), and are given by the color equations

$$[(V_{606} - i_{775}) > 1.5 + 0.9 \times (i_{775} - z_{850})] \vee \vee [(V_{606} - i_{775}) > 2.0] \wedge (V_{606} - i_{775}) \geqslant 1.2 \wedge (i_{775} - z_{850}) \leqslant 1.3 \wedge [(\mathrm{S/N})_B < 2] \quad (1.2)$$

and

$$(i_{775} - z_{850}) > 1.3 \wedge [(\mathrm{S/N})_B < 2] \vee [(\mathrm{S/N})_V < 2], \quad (1.3)$$

respectively (see Figure 2 for a collapsed representation of the selection windows for V_{606}- and i_{775}-band dropouts). For all three selection criteria above, when the isophotal signal-to-noise ratio (S/N) in a given band is less than 1, limits on the colors have been calculated using the 1σ error on the isophotal magnitude.

We have restricted the photometric samples to galaxies with isophotal S/N $\geqslant$ 5 in the z_{850} band, and we have visually inspected each candidate, removing sources that were deemed artifacts. In addition, we have estimated the number of spurious detections using counts of negative sources detected in the same data set. Together, these amount to a negligible number of spurious sources for the B_{435}- and V_{606}-dropout samples, and $\approx$12% for the i_{775} dropouts. We have also eliminated all sources with stellar morphology down to apparent magnitude $z_{850} \sim 26$, i.e., where such a morphological classification is reliable. This accounts for an additional 3.1%, 8.3%, and 4.6% of the B_{435}-, V_{606}- , and i_{775}-dropout samples, respectively. While this procedure biases our samples against LBGs (and high-redshift quasars) that are unresolved by ACS, it minimizes contamination from Galactic stars. Note that we have spectroscopically observed a few pointlike sources that obey the dropout selections in order to verify that such sources are indeed Galactic. In practice, these cullings of the dropout samples result in negligible changes to the spectroscopic samples and to key measured quantities, such as the specific luminosity density.

Down to $z_{850} \leqslant 26.5$, roughly the 50% completeness limit for unresolved sources, the culled samples include 1544, 490, and 213 B_{435}-, V_{606}-, and i_{775}-band dropouts, respectively. With a survey area of 316 arcmin^2, this corresponds to surface density $\Sigma = 4.89 \pm 0.12$, 1.55 ± 0.07, and 0.67 ± 0.05 galaxies per arcmin^2 for the three types of dropouts, respectively. Error bars simply reflect Poisson fluctuations.

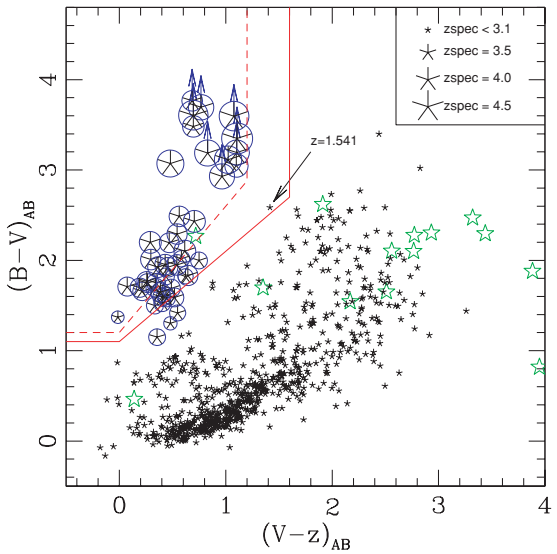

Figure 1. Color–color diagram for the selection of B_{435}-band dropout galaxies, the solid line outlines the region of the selection. The black "skeletal" symbols with fixed size are all sources in the FORS2 sample in the redshift range $0 < z < 3.1$, those with redshift in the range $3.1 < z < 4.4$ are plotted varying the symbol size accordingly with the spectroscopic redshift value. Stars have been marked with "star" green symbols. Galaxies confirmed in the redshift interval $3.1 < z < 4.4$ have been marked with open circles. The arrows mark 1σ lower limit of the colors. The one low-z galaxy identified at $z = 1.541$ has been marked with an arrow (see the text for details).

(A color version of this figure is available in the online journal.)

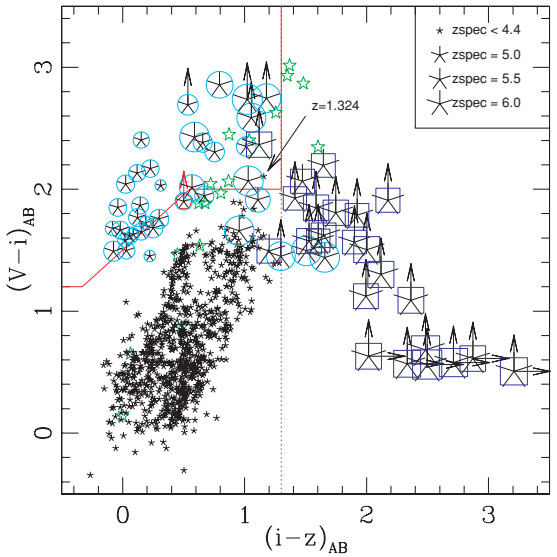

Figure 2. Color–color diagram for the selection of V_{606}-band dropout galaxies and i_{775}-band dropout ones, the solid line outlines the region of the V_{606}-band dropout selection, while the vertical dotted line outlines the i_{775}-band dropout region (i_{775}–$z_{850} > 1.3$). The black "skeletal" symbols with fixed size are all sources in the FORS2 sample in the redshift range $0 < z < 4.4$, those with redshift in the range $4.4 < z < 6.5$ are plotted varying the symbol size accordingly with the spectroscopic redshift value. Galaxies confirmed in the redshift interval $4.4 < z < 5.6$ have been marked with open circles and those with $z > 5.6$ have been marked with open squares. Stars have been plotted with "star" green symbols. The open pentagon marks a serendipitously discovered galaxy ($z = 4.783$ QF = C, see the text). The arrows mark 1σ lower limit of the colors. The one low-z galaxy identified at $z = 1.324$ has been marked with an arrow (see the text for details).

(A color version of this figure is available in the online journal.)

We note that while the V_{606}- and i_{775}-band dropout samples are mutually exclusive (i.e., $i_{775} - z_{850} \leqslant 1.3$ vs. $i_{775} - z_{850} > 1.3$,

respectively), the intersection of the B_{435}- and V_{606}-band dropout samples may be nonzero. However, in this latter case, no sources in common have been found down to the $z_{850} \leqslant 26.5$, and only one galaxy satisfies both criteria when the magnitude limit is extended down to $z_{850} \leqslant 27.5$ (i.e., GDS J033245.88−274326.3).

We have used Monte Carlo simulations to estimate the redshift distribution function of our LBG samples and compared the results to observations. The technique is the same as that used in G04b and consists of generating artificial LBGs distributed over a large redshift range (we used $2.5 \leqslant z \leqslant 8$) with assumed distribution functions for UV luminosity (we used a flat distribution, discussed below), SED, morphology, and size. We adjusted the input SED and size distribution functions by requiring that the distribution functions recovered from the simulations match the $z \sim 4$ observed sample, the largest of the three GOODS samples. In this way, both simulations and observations are subject to similar incompleteness, photometric errors (in flux and color), blending, and other measurement errors. The model SED used for the simulations is based on a synthetic spectrum of a continuously star-forming galaxy with age 10^8 yr, Salpeter IMF, and solar metallicity (Bruzual & Charlot 2003). We reddened it with the starburst extinction law (Calzetti et al. 2000) and $E(B-V)$ randomly extracted from a Gaussian distribution with $\mu_{E(B-V)} = 0.15$ and $\sigma_{E(B-V)} = 0.15$. In other words, the dispersion of the LBG UV SEDs is modeled as only due to the dispersion in the amount of obscuration for the same unobscured SED, neglecting the effects of age and metallicity of the stellar populations. This is obviously a crude approximation, but, thanks to the strong degeneracy between age, obscuration, and metallicity on the broadband UV colors of star-forming galaxies, it is adequate here since we are only interested in measuring the selection effects due to the specifics of the observations. For the cosmic opacity, we have adopted the Madau (1995) prescription, extrapolated to higher redshifts when necessary. To model the dispersion of the morphologies of the galaxies, we have used an equal number of $r^{1/4}$ and exponential profiles with random orientation, and size extracted from a log-normal distribution function (see Ferguson et al. 2004). We found the average redshift and standard deviation of the redshift distribution to be $z_B = 3.78$ and $\sigma_B = 0.34$ for the B_{435}-dropout sample, $z_V = 4.92$ and $\sigma_V = 0.33$ for the V_{606}-dropout sample, and $z_i = 5.74$ and $\sigma_i = 0.36$ for the i_{775}-dropout sample.

2.3. The Spectroscopic Sample

We have selected a sample of 202 LBGs from the three samples defined above as primary targets of the FORS2 spectroscopic observations. While the criteria to include a galaxy in the target list were mostly based on its apparent magnitude, as we detail below, we did not set a strict flux limit for the spectroscopic sample in these initial high-redshift LBG spectroscopic studies. This allowed us to empirically assess how often the presence of Lyα emission allows the measurement of the redshift of galaxies which are too faint for absorption spectroscopy.

Targets were assigned slits in the FORS2 multiobject spectroscopic masks according to an algorithm in which two competing factors combine to maximize (1) the number of targets and (2) the likelihood of success, under the assumption that brighter targets are more likely to result in successful identifications. In practice, while brighter galaxies were more likely to be assigned a slit, (slightly) fainter targets could still win the competition if their coordinates allowed a larger total number of targets on a given mask. Relatively faint targets in close proximity to brighter one were also assigned a slit if their inclusion could be made without penalty. Where possible, we assigned faint targets to multiple masks.

When the number of available slits in a mask exceeded that of available targets, we populated the remaining slits with "filler" targets selected to test target-selection criteria and to identify lower redshift galaxies in the range $z \sim 1$–2 (for a summary of the global target selection of the FORS2 campaign, see Vanzella et al. 2006). In particular, we selected some filler targets using LBG criteria that extended the primary B_{435}- and V_{606}-band dropout-selection criteria to galaxies with less pronounced "Lyman drops" and bluer UV continuum, thus getting closer to the locus of general field galaxies. As discussed earlier, such observations are useful for exploring the dependence of the redshift distribution function of the confirmed LBGs on the details of the color selection, as well as for measuring contamination by low-redshift interlopers. In what follows, we refer to these more loosely defined B_{435}- and V_{606}-band dropouts simply as "fillers." Only three such spectroscopically identified fillers are considered below, two B_{435}-dropout fillers (GDS J033234.40−274124.3 at $z = 3.418$, QF = B and GDS J033251.81−275236.5 at $z = 3.468$, QF = A) and one V_{606}-dropout filler (GDS J033239.82−275258.1 at $z = 5.543$, QF = C). We will report more extensively on these tests in following papers, which will also include spectroscopic observations of GOODS galaxies obtained with different instrumental configurations.

3. FORS2 SPECTROSCOPIC OBSERVATIONS

The details of the observations, including journals of the observing runs, data reduction, the extractions of the spectra have been reported in Vanzella et al. (2005, 2006, 2008), and we refer the reader to those papers. We recall that the wavelength coverage was typically 5700–10000 Å with a spectral resolution of $R = \lambda/\Delta\lambda = 660$, corresponding to 13 Å at 8600 Å. No order separation filter was used.

In the vast majority of cases, the redshift has been calculated through the identification of prominent features of LBG spectra, e.g., Lyα either in emission or absorption, and Si II 1260 Å, O I+Si II 1302 Å (a blend at the spectral resolution of our instrumental setup), C II 1335 Å, Si IV 1394,1403 Å, Si II 1527 Å, C IV 1548,1551 Å in absorption.

Redshift determinations have been made based on visual identification of spectral features as well as by cross correlating the observed spectra against high-fidelity LBG templates of differing spectral types using the *rvsao* package in the IRAF environment. In particular, we used emission and absorption line LBG templates from Shapley et al. (2003) as well as the lensed absorption line LBG cB58 (Pettini et al. 2000). Each two-dimensional spectrum has been visually inspected, including consideration of its slit orientation on the sky. In many cases where no continuum has been detected, we derive a redshift measurement from Lyα emission.

We have co-added all repeated spectra to improve the final S/N. The typical exposure time for each mask was about 14,400 s and for co-added sources, total exposure times range from 20,000 to 80,000 s (e.g., see Vanzella et al. 2008).

We have assigned each measured redshift a quality flag (QF), with values of either A (unambiguous identification), B (likely identification; e.g., based on only one line or a continuum break), or C (uncertain identification). The presence of Lyα emission in the second-order spectrum (at greater than 10000 Å) has

also been used on occasion, especially for faint sources with low QFs based on absorption features. For example, one B_{435}-band dropout source (GDS J033221.05−274820.5) shows an apparently featureless continuum with a second-order emission line at ∼10400 Å, implying $z \sim 3.3$. Indeed, recently the VIMOS spectroscopic observations have confirmed this galaxy to be at $z = 3.385$ (Popesso et al. 2009).

We have assigned a redshift to 118 galaxies of the initial list of 202 targets, or 58.4% of the input list; this relatively low success rate is, in large part, due to two factors: (1) the target list includes a relatively large fraction of faint sources—65% or 32.2% of the sample have $z_{850} > 26$; and (2) the difficulty in deriving redshifts for galaxies at $z < 3.6$ with our instrumental configuration. In the latter case, depending on the slit position, Lyα and the UV absorption features are often blueward of the spectral range available.

Of the 118 spectroscopically identified sources, 106 have redshifts in the expected range for their adopted color selection. Note that some of these redshifts have already been published in Vanzella et al. (2005, 2006). Of the sources outside the expected redshift range, one source is a low-redshift galaxy from the B_{435}-band dropout sample, one is a low-redshift galaxy from the V_{606}-band dropout sample, and 10 are Galactic stars (1, 3, and 6 from the B_{435}-, V_{606}-, and i_{775}-dropout samples, respectively). We note that one faint star, GDS J033238.80−274953.7 ($z_{850} = 25.16$), that we spectroscopically classify with QF = C, has been confirmed Galactic in nature due to the detection of its proper motion (M. Stiavelli 2008, private communication). Excluding the Galactic stars and the two low-redshift interlopers, the final list of spectroscopically identified LBGs includes 46 B_{435}-band dropouts, 32 V_{606}-band dropouts, and 28 i_{775}-band dropouts (reported in Tables 1, 2, and 3).

As mentioned above, we have assigned redshifts to three high-redshift filler targets found to be in the same redshift range as the primary LBG sample. This brings the total number of high-redshift ($z > 3.1$) spectroscopic identifications to 109, of which 32 have QF = C. Of these 109 galaxies, 70 have redshift $z > 4$ (24 with QF = C); 37 have redshift $z > 5$ (13 have QF = C); and 32 have redshift $5.5 < z < 6.5$ (11 with QF = C; see Table 4 for a summary).

Finally, we also found five serendipitously identified, high-redshift galaxies. These fell, as second or third sources, on slitlets assigned to other primary targets. For four of them, the redshift identification relies upon an Lyα emission line; only in one case does the redshift rely upon absorption features. These five serendipitous sources are, in right ascension order, as follows.

1. GDS J033218.27−274712.0, at $z = 4.783$ (QF = C), marked in Figure 2 with a red pentagon, is close to the V_{606}-band dropout selection window (V_{606}–$i_{775} > 1.901$, i_{775}–$z_{850} = 0.501$).
2. GDS J033219.41−274728.4, at $z = 3.250$ (QF = C). This galaxy shows a flat continuum and an absorption doublet interpreted as C IV 1548,1551 Å.
3. GDS J03322.89−274521.0, at $z = 5.128$ (QF = C). This source, clearly visible in the i_{775} band (from which the coordinates were measured) is not detected in the B_{435}, V_{606}, or z_{850} bands. We assume that the emission line is Lyα, though lacking firm constraints on the continuum SED, we cannot rule out another interpretation such as [O II]3727 at redshift $z = 0.999$. This source is not used in the following analysis.
4. GDS J033228.94−274128.2, at $z = 4.882$ (QF = B), is discussed in Vanzella et al. (2005, see their Figure 13). The source is not present in the ACS catalogs because of blending with a bright galaxy.
5. GDS J033243.16−275034.6, at $z = 4.838$ (QF = C), is discussed in Vanzella et al. (2006, see their Figure 2, top panel). This source is not present in the ACS catalogs because of blending with a bright star.

Figures 3 and 4 show the one-dimensional spectra for all confirmed LBGs, separated depending on whether Lyα is in emission or absorption. Figure 5 shows the two-dimensional spectra of confirmed LBGs at $z > 5$. Table 4 summarizes the characteristics of each dropout sample compared with those expected from the Monte Carlo simulations of the redshift selection described in Section 2.2, while Figure 6 shows the observed redshift distribution of each dropout category. Note the (small) overlap between the redshift distribution functions for B_{435}- and V_{606}-band dropouts at $z \sim 4.5$ and between V_{606}- and i_{775}-band dropouts at $z \sim 5.5$.

4. EFFICIENCY OF THE PHOTOMETRIC SELECTIONS

The effectiveness of the LBG color selection has been verified at $z \sim 3$ by means of an extensive program of spectroscopic confirmations of over a thousand U-band dropouts (Steidel et al. 2003). At higher redshift, the spectroscopic samples of LBGs collected by various groups (e.g., Steidel et al. 1999; Vanzella et al. 2006, 2008; Popesso et al. 2009; Yoshida et al. 2006; Ando et al. 2007) are rather small and estimates of successful identification rates for a given set of color criteria remain correspondingly uncertain. Details of the filters and color criteria used by various surveys can result in different relative proportions of successfully identified LBGs (i.e., in the targeted redshift range), interlopers (i.e., outside of the targeted redshift range), as well as other types of unwanted sources (e.g., active galactic nucleus in the targeted redshift range). The GOODS data set is being widely used for a variety of studies of the properties of galaxies at high redshifts (e.g., Bouwens et al. 2007), and many of these studies use samples of photometrically selected, high-redshift galaxies from the GOODS ACS data without spectroscopic verification of the effective composition of the samples. Even under the most optimistic assumption that the samples include negligible fractions of interlopers and unwanted sources, fundamental quantities such as the shape of the redshift distribution, which is important for the measures of the spatial clustering and luminosity function, remain largely unknown.

The spectroscopic sample obtained with FORS2 discussed here is our initial effort to characterize the effectiveness of the GOODS LBG color-selection criteria in selecting star-forming galaxies at high redshifts; the numbers cited below are summarized in Table 4.

Of the 85 B_{435}-band dropout candidates selected for spectroscopic observations, we have secure redshifts for 48 sources down to $z_{850} = 25.5$ (56%). Of the 48 identifications, 46 have redshifts in the expected range for B_{435}-band dropouts, and only two are foreground objects. One is a Galactic star (QF = B, z_{850}=23.43, SExtractor stellarity index S/G = 0.99, from SExtractor algorithm; Bertin & Arnouts 1996) and the other is a galaxy at $z = 1.541$ identified from [O II]3727 emission (QF = B, z_{850}=25.49).[12] We have classified eight of the 48 identifications as having QF = C. Assuming that all the identifications

[12] This galaxy is well detected in the V_{606}, i_{775}, and z_{850} bands (with S/N of

Table 1
The Spectroscopic Sample of the B_{435}-Band Dropouts

GOODS ID	z	QF	Class	z_{850}	h.l.r.	S/G	$(B_{435}-V_{606})$	$(V_{606}-z_{850})$	$(S/N)_B$
J033200.31−274250.7	0.000	B	star	23.43	2.65	0.99	2.27	0.72	15.72
J033239.12−274751.6	1.541	B	em.	25.49	4.14	0.16	2.59	1.42	1.02
J033242.84−274702.5[a]	3.193	B	em.	24.92	3.07	0.96	1.37	−0.01	17.00
J033234.83−275325.2	3.369	B	abs.	24.24	9.65	0.03	1.82	0.62	7.19
J033220.85−275038.9	3.450	B	abs.	24.56	14.09	0.00	2.02	0.58	3.73
J033223.34−275156.9	3.470	A	abs.	23.35	5.52	0.03	2.00	0.75	12.30
J033223.22−275157.9	3.470	A	abs.	25.07	6.75	0.03	1.50	0.33	7.31
J033214.82−275204.6	3.473	A	comp.	24.14	8.19	0.03	1.53	0.40	16.71
J033235.06−275234.6	3.477	C	comp.	25.12	8.28	0.03	1.61	0.43	6.15
J033220.97−275022.3	3.478	A	abs.	24.70	8.86	0.03	1.82	0.44	5.84
J033225.16−274852.6	3.484	A	comp.	24.05	6.73	0.03	1.58	0.45	14.76
J033223.99−275216.1	3.557	B	comp.	25.15	7.06	0.03	1.59	0.40	6.81
J033226.76−275225.9	3.562	A	abs.	24.10	6.69	0.03	1.69	0.49	12.64
J033229.02−274234.0	3.585	B	abs.	25.01	5.66	0.03	1.66	0.21	10.59
J033220.94−274346.3*	3.596	A	em.	24.61	6.37	0.45	1.75	0.34	9.53
J033229.14−274852.6	3.597	A	em.	24.60	4.69	0.03	1.70	0.34	11.64
J033201.84−274206.6	3.603	A	em.	25.04	6.50	0.01	1.71	0.07	9.50
J033242.50−274551.7	3.604	A	em.	24.24	7.59	0.04	1.75	0.27	9.35
J033217.13−274217.8	3.617	A	em.	25.11	4.20	0.36	1.70	0.19	9.11
J033235.96−274150.0	3.618	A	comp.	24.11	4.36	0.03	1.65	0.39	16.16
J033215.78−274145.6	3.646	C	abs.	24.79	5.69	0.48	1.92	0.46	6.47
J033217.22−274754.4*	3.652	A	em.	24.84	3.45	0.33	1.77	0.26	11.10
J033222.59−275118.0	3.660	A	abs.	25.10	6.49	0.03	2.20	0.47	4.25
J033245.57−275333.3	3.685	A	abs.	24.61	4.90	0.03	1.83	0.64	7.02
J033217.66−275332.0*	3.696	B	em.	24.29	5.43	0.02	2.29	0.54	7.27
J033232.08−274136.4	3.697	B	abs.	24.74	7.30	0.03	2.49	0.56	3.68
J033230.10−275057.7	3.704	A	comp.	24.64	15.14	0.02	1.95	0.43	3.78
J033226.28−275245.7	3.705	B	comp.	24.65	7.07	0.32	2.01	0.30	6.93
J033218.05−274519.0	3.706	A	abs.	24.61	13.03	0.02	3.79	0.68	0.96
J033219.81−275300.9	3.706	A	comp.	24.50	5.82	0.03	1.95	0.54	8.10
J033219.60−274840.0	3.708	A	em.	25.30	4.28	0.40	1.93	0.36	5.67
J033225.82−274250.3	3.770	C	abs.	25.00	7.43	0.03	3.48	0.70	1.01
J033233.33−275007.4	3.791	A	em.	24.84	4.50	0.05	2.20	0.29	5.50
J033234.65−274115.4	3.794	C	abs.	24.62	7.66	0.02	2.43	0.70	2.54
J033236.83−274558.0	3.797	A	comp.	24.58	5.59	0.29	2.10	0.61	5.54
J033239.67−274850.6*	3.887	B	abs.	24.56	5.15	0.03	3.05	1.10	1.57
J033238.73−274413.3	4.000	C	abs.	24.81	11.18	0.00	2.95	0.96	−0.21
J033227.94−274618.6	4.000	C	abs.	25.23	4.23	0.03	3.21	1.10	−1.38
J033246.25−274847.0	4.020	A	abs.	24.88	5.09	0.03	3.71	0.77	0.82
J033241.16−275101.5	4.058	B	abs.	25.25	7.20	0.03	3.21	0.83	0.16
J033240.38−274431.0	4.120	A	em.	25.24	3.45	0.64	3.07	0.48	2.20
J033234.35−274855.8	4.142	A	comp.	24.11	10.37	0.03	3.11	1.02	1.66
J033218.26−274802.5	4.280	A	abs.	24.65	4.35	0.05	3.62	1.08	−0.75
J033212.98−274841.1*	4.283	B	em.	24.70	7.81	0.03	3.63	0.69	−0.29
J033248.24−275136.9	4.374	A	em.	24.87	4.81	0.09	3.37	1.11	−0.54
J033214.50−274932.7	4.738	C	em.	25.40	5.30	0.30	3.00	0.96	−0.08
J033257.17−275145.0	4.760	A	em.	24.64	5.52	0.02	2.71	1.53	1.47

Notes. The redshift reported is the result of the cross correlation between the spectrum and the reference template. In the first four columns, the GDS name, the redshift value, QF, and class, are listed, respectively. Columns 5–10 are the z_{850} AB magnitude (MAGAUTO), the h.l.r., the galaxy–star classifier (0: galaxy; 1: pointlike source), the $(B_{435}-V_{606})$ and the $(V_{606}-z_{850})$ colors, and the isophotal S/N in the B_{435} band (if less than 1, the $(B_{435}-V_{606})$ color is a lower limit).

[a] It has been identified with broad Mg II in emission, QSO.

* For these sources, the QF has been improved (i.e., C to B or B to A) to respect the online release of Vanzella et al. (2008), after re-analyzing the whole LBG sample.

with QF = C are correct, the efficiency of the B_{435}-band dropout selection is $46/48 = 96\%$. Omitting the two foreground sources, the mean and rms of the B_{435}-band dropout redshift distribution are $\langle z \rangle = 3.765$ and $\sigma_z = 0.328$, respectively, fully consistent with the prediction from Monte Carlo simulations (see Section 2.2 and Table 4).

Figure 1 shows the $(B_{435}-V_{606})$ versus $(V_{606}-z_{850})$ color–color diagram for the entire FORS2 spectroscopic sample. The region of B_{435}-band dropout sources is marked with a solid line and the size of the symbols scale linearly with redshift for sources at $z > 3.1$; at redshift lower than 3.1, the size of the symbol is fixed. The majority of the galaxies with $z > 3$ lie in the B_{435}-band dropout region. It is evident from Figure 1 that the lower tail of the redshift distribution is

13.9, 14.1, and 26.1, respectively). This fact excludes the Lyα possibility at redshift ∼6.8. Other possible emission lines are [O III]5007 and/or Hβ at $z \sim 0.9$; however, in this case, the [O II]3727 should be detected at 7049 Å, region free from skylines. If we assume Hα line, we should expect to observe at least Hβ at 7014 Å. Therefore, the most probable interpretation is [O II]3727 at $z = 1.541$.

Table 2
The Spectroscopic Sample of the V_{606}-Band Dropouts

GOODS ID	z	QF	Class	z_{850}	h.l.r.	S/G	$(V_{606}-i_{775})$	$(i_{775}-z_{850})$	$(S/N)_V$
J033242.08−274911.6	0.000	B	star	23.43	2.88	0.98	2.63	1.25	6.34
J033224.11−274102.1	0.000	A	star	23.39	2.61	0.99	2.45	0.87	12.10
J033237.69−275446.4	0.000	A	abs.	23.60	2.68	0.99	2.40	1.04	9.42
J033220.31−274043.4	1.324	B	abs.	24.09	10.18	0.00	2.10	1.16	3.40
J033242.62−275429.0	4.400	C	abs.	25.61	6.60	0.02	2.03	0.31	4.11
J033222.88−274727.6	4.440	B	abs.	24.92	4.05	0.03	1.63	0.09	14.73
J033222.97−274629.1	4.500	C	abs.	25.34	6.91	0.02	1.72	0.19	6.63
J033228.56−274055.7	4.597	B	abs.	25.44	7.53	0.00	1.58	0.02	9.29
J033216.98−275123.2	4.600	B	abs.	25.30	6.56	0.03	1.68	−0.08	9.02
J033255.08−275414.5	4.718	A	em.	24.83	7.11	0.01	2.40	0.15	5.77
J033247.58−275228.2	4.758	C	em.	25.73	8.33	0.01	1.87	0.14	4.28
J033229.29−275619.5[a]	4.762	A	em.	25.05	2.76	0.99	1.65	0.15	12.95
J033243.53−274919.2	4.763	A	em.	25.56	4.89	0.02	2.13	0.12	5.13
J033240.12−274535.5	4.773	B	em.	25.55	6.23	0.02	1.62	0.06	7.24
J033221.93−274533.1	4.788	C	abs.	25.82	4.86	0.04	2.17	0.23	3.56
J033228.85−274132.7	4.800	B	em.	25.43	4.50	0.03	1.66	−0.02	9.84
J033205.26−274300.4	4.804	A	em.	25.24	4.11	0.03	1.85	−0.04	11.39
J033210.03−274132.7	4.811	A	em.	25.03	3.63	0.31	1.77	0.12	12.63
J033242.66−274939.0	4.831	B	em.	26.08	3.55	0.60	2.04	0.02	4.69
J033233.48−275030.0	4.900	C	abs.	25.76	4.07	0.07	2.38	0.66	2.65
J033223.99−274107.9	4.920	C	abs.	25.26	2.38	0.98	2.31	0.75	4.51
J033247.66−275105.0*	4.920	C	abs.	25.55	2.57	0.98	2.35	1.01	2.66
J033234.49−274403.0	4.948	C	em.	26.04	3.45	0.51	1.49	−0.08	9.19
J033225.32−274530.9	4.992	B	em.	26.70	4.45	0.11	2.69	0.53	0.55
J033221.30−274051.2	5.292	A	em.	25.23	5.36	0.10	2.01	0.57	3.58
J033245.43−275438.5	5.375	A	em.	25.15	6.08	0.03	2.86	0.79	1.94
J033224.40−275009.9	5.500	C	abs.	25.29	7.76	0.02	2.74	1.18	−0.07
J033237.63−275022.4	5.518	A	em.	25.76	8.05	0.01	2.58	1.05	0.80
J033218.92−275302.7	5.563	A	em.	24.58	3.37	0.83	2.43	0.59	6.28
J033211.93−274157.1	5.578	B	em.	26.53	4.10	0.10	2.07	1.03	1.40
J033245.23−274909.9	5.583	B	em.	25.81	6.97	0.01	2.73	1.02	0.10
J033214.74−274758.7	5.939	B	em.	26.36	4.15	0.17	2.36	1.12	−0.17

Notes. Columns as described in Table 1.
[a] Identify with Lyα and NV1240 Å (and possibly C IV 1549 Å), QSO.
* For this source, the QF has been changed (B to C) to respect the online release of Vanzella et al. (2008), after re-analyzing the whole LBG sample.

located in the lower part of the selection region: the eight sources with $3.1 < z < 3.5$ have a mean $(B_{435}-V_{606}) = 1.69 \pm 0.23$ and $(V_{606}-z_{850}) = 0.44 \pm 0.21$. In this redshift range, the selection criteria are more uncertain and depend on the intrinsic properties of the sources. Photometric errors may also scatter sources across the boundary of the selection region.

For the sample of V_{606}-band dropouts, we have assigned spectroscopic slits to 52 candidates and derived a redshift identification for 36 of them (69%) down to z_{850}= 26.7, of which 11 have been given QF = C. Among the confirmed redshifts, 32 are in the range expected for V_{606}-band dropouts (11 with QF = C), three are Galactic stars (all of them with $z_{850}\sim$ 23.5 and S/G = 0.99), and one, GDS J033220.31−274043.4, is a low-redshift interloper at $z = 1.324$ (QF = B).[13] Assuming that all of the QF = C identifications are correct, the efficiency of the $z \sim 5$ LBG selection is 32/36 = 89%; omitting the foreground sources, the mean and rms of the redshift distribution are $\langle z \rangle = 4.962$ and $\sigma_z = 0.386$, respectively. Again, the observed redshift distribution agrees well with the Monte Carlo predictions (Table 4).

Figure 2 shows the $(V_{606}-i_{775})$ versus $(i_{775}-z_{850})$ color–color diagram for the entire FORS2 spectroscopic sample. The selection window for the V_{606}-band dropouts (solid lines) and i_{775}-band dropouts (dotted line; $i_{775}-z_{850} > 1.3$) are plotted. Galaxies confirmed in the redshift interval $4.4 < z < 5.6$ are marked with open circles. The majority of galaxies at $z > 4.4$ are located within the selection regions.

Finally, of the 65 i_{775}-band dropouts selected for spectroscopic observations, we have secured redshifts for 34 down to $z_{850} = 27.4$ (52%). Of these, 28 have redshifts in the range $5.5 < z < 6.3$, of which 23 are based on the identification of an observed emission line as redshifted Lyα (seven have QF = C) and five are based on the identification of an observed continuum break as the onset of the high-redshift Lyα forest (four have QF = C and one has QF = B). The remaining six i_{775}-band dropouts are Galactic stars (four with QF = C and two with QF = B; all with stellarity index S/G > 0.91 and $z_{850}<$ 25.4). Assuming that all of the QF = C identifications are correct, the efficiency of the $z \sim 6$ LBG selection is thus 28/34 = 82%. The average redshift and standard deviation of the successfully identified i_{775}-band dropouts are $\langle z \rangle = 5.898$ and $\sigma_z = 0.184$. While the average of the distribution is consistent with the

[13] This galaxy is interesting in its own right. It has colors $(V_{606}-i_{775}) = 2.077$ and $(i_{775}-z_{850}) = 1.246$ and falls in the upper right portion of the selection region in Figure 2. A pronounced break around 4000 Å and the Ca II HK absorption lines are evident in the spectrum, but there is no [O II]3727 emission line identified down to a 3σ of 2×10^{-18} erg s^{-1} cm^{-2} Å^{-1}, suggesting that the emission is dominated by evolved stellar populations with little or no star formation activity.

Table 3
The Spectroscopic Sample of the i_{775}-Band Dropouts

GOODS ID	z	QF	Class	z_{850}	h.l.r.	S/G	$(i_{775}-z_{850})$	$(S/N)_i$
J033219.23−274545.5	0.000	C	star	23.47	2.64	0.98	1.35	37.91
J033218.19−274746.6	0.000	B	star	23.76	2.66	0.99	1.48	28.00
J033224.79−274912.9	0.000	C	star	24.95	2.77	0.99	1.60	10.92
J033238.80−274953.7	0.000	C	star	25.16	3.81	0.91	3.87	0.99
J033222.47−275047.4	0.000	C	star	24.42	2.70	0.99	1.74	15.04
J033238.02−274908.4	0.000	B	abs.	25.41	2.59	0.99	1.37	9.77
J033239.03−275223.1**	5.559	C	em.	25.72	4.08	0.18	1.66	5.16
J033215.90−274123.9	5.574	B	em.	25.48	8.31	0.00	1.51	4.56
J033227.91−274942.0	5.757	C	em.	26.91	3.48	0.27	1.60	2.45
J033255.32−275315.6	5.764	B	em.	26.15	8.21	0.01	1.41	3.53
J033225.61−275548.7[a]	5.786	A	em.	24.69	3.69	0.64	1.65	11.87
J033246.04−274929.7[b]	5.787	A	em.	26.11	4.12	0.02	1.92	3.06
J033254.10−274915.9	5.793	C	em.	25.26	10.84	0.00	1.90	2.52
J033240.01−274815.0[c]	5.828	A	em.	25.34	3.95	0.39	1.47	7.92
J033233.19−273949.1*	5.830	B	abs.	25.41	6.74	0.01	2.18	3.30
J033249.98−274656.2	5.890	B	em.	26.25	3.47	0.50	1.65	3.76
J033224.97−275613.7	5.899	B	em.	26.78	4.10	0.07	1.99	1.75
J033239.06−274538.7	5.920	B	em.	27.05	3.80	0.90	1.53	2.45
J033228.19−274818.7	5.940	B	em.	26.48	3.97	0.18	1.59	3.08
J033215.76−274817.2	5.944	C	em.	26.09	5.08	0.17	1.75	3.01
J033236.47−274641.4[d]	5.950	C	abs.	26.30	4.69	0.01	2.88	0.58
J033232.46−274001.9	5.977	B	em.	26.51	3.59	0.28	2.36	1.51
J033218.08−274113.1	5.979	C	em.	26.72	5.61	0.00	2.03	0.27
J033224.80−274758.8	5.996	B	em.	26.06	5.64	0.03	2.00	2.33
J033229.33−274014.3	6.000	C	abs.	26.81	2.77	0.90	2.12	1.90
J033246.43−275524.4	6.082	B	em.	26.80	4.68	0.75	2.35	0.15
J033223.84−275511.6	6.095	B	em.	26.31	3.08	0.67	3.22	−0.27
J033229.84−275233.2	6.197	B	em.	26.26	7.52	0.25	2.48	1.16
J033222.28−275257.2	6.200	C	abs.	25.86	6.31	0.27	2.73	−0.01
J033217.81−275441.6	6.277	B	em.	26.87	2.75	0.94	2.51	0.62

Notes. Columns as described in Table 1.
[a] Also known as SBM03 3 (Stanway et al. 2003; Bunker et al. 2003).
[b] Also known as GLARE 3001 (Stanway et al. 2004b).
[c] Also known as SiD002 (Dickinson et al. 2004), GLARE 1042 (Stanway et al. 2004b), SBM03 1 (Stanway et al. 2003).
[d] This has been identified by Malhotra et al. (2005) in the HUDF with ACS grism spectra.
* For this source, the QF has been changed (C to B) to respect the online release of Vanzella et al. (2008), after re-analyzing the whole LBG sample.
** Redshift has been added to the previous LBG list (Vanzella et al. 2008), after re-analyzing the whole LBG sample and tacking together the unconclusive single spectra.

Table 4
Fraction of Confirmed Dropout Candidates, "Nobs." Indicates the Number of Candidates Observed

Classes	Nobs.	High-z $N^{(em,abs,comp)}_{(A,B,C)}$	Low-z $N^{(em,abs,comp)}_{(A,B,C)}$	Measured[a] $\langle z\rangle\pm\sigma$	Expected[a,b] $\langle z\rangle\pm\sigma$	Compl.[a]
B_{435}-drop	85	$46^{(15,21,10)}_{(27,11,8)}$	$2^{(1,1,0)}_{(0,2,0)}$	3.76 ± 0.33	3.78 ± 0.34	5%
V_{606}-drop	52	$32^{(19,13,0)}_{(9,12,11)}$	$4^{(0,4,0)}_{(2,2,0)}$	4.96 ± 0.38	4.92 ± 0.33	14%
i_{775}-drop	65	$28^{(24,4,0)}_{(3,13,12)}$	$6^{(0,6,0)}_{(0,2,4)}$	5.90 ± 0.18	5.74 ± 0.36	29%
Fillers	...	$3^{(1,2,0)}_{(1,1,1)}$	...	$3.4 < z < 5.5$	...	...
Serend.	...	$5^{(4,1,0)}_{(0,1,4)}$	...	$3.2 < z < 5.8$	...	...
Sum	202	114	12			

Notes. The number of confirmed high- and low-redshift galaxies is reported in columns 3 and 4, respectively (with the fraction of "em.," "abs.," and "comp." classes and the fraction of QFs "A," "B," and "C"). In columns 5 and 6, the average and standard deviation of the redshift distribution for the confirmed high-z sample are shown. In column 7, the completeness is reported.
[a] Calculated down to $z_{850} = 26.5$.
[b] See Giavalisco et al. (2004b).

predicted one, we note that the standard deviation is almost a factor of 2 narrower. This may be an indication of large-scale structure at this redshift; from ACS grism spectroscopy, Malhotra et al. (2005) note the structure at this same mean redshift in the HUDF.

We note that several sources from our i_{775}-dropout spectroscopic sample were previously published, including spectroscopic observations. One has a well-observed spectrum showing Lyα emission at $z = 5.829$ (Stanway et al. 2004b; Dickinson et al. 2004; Bunker et al. 2004). An additional two sources were

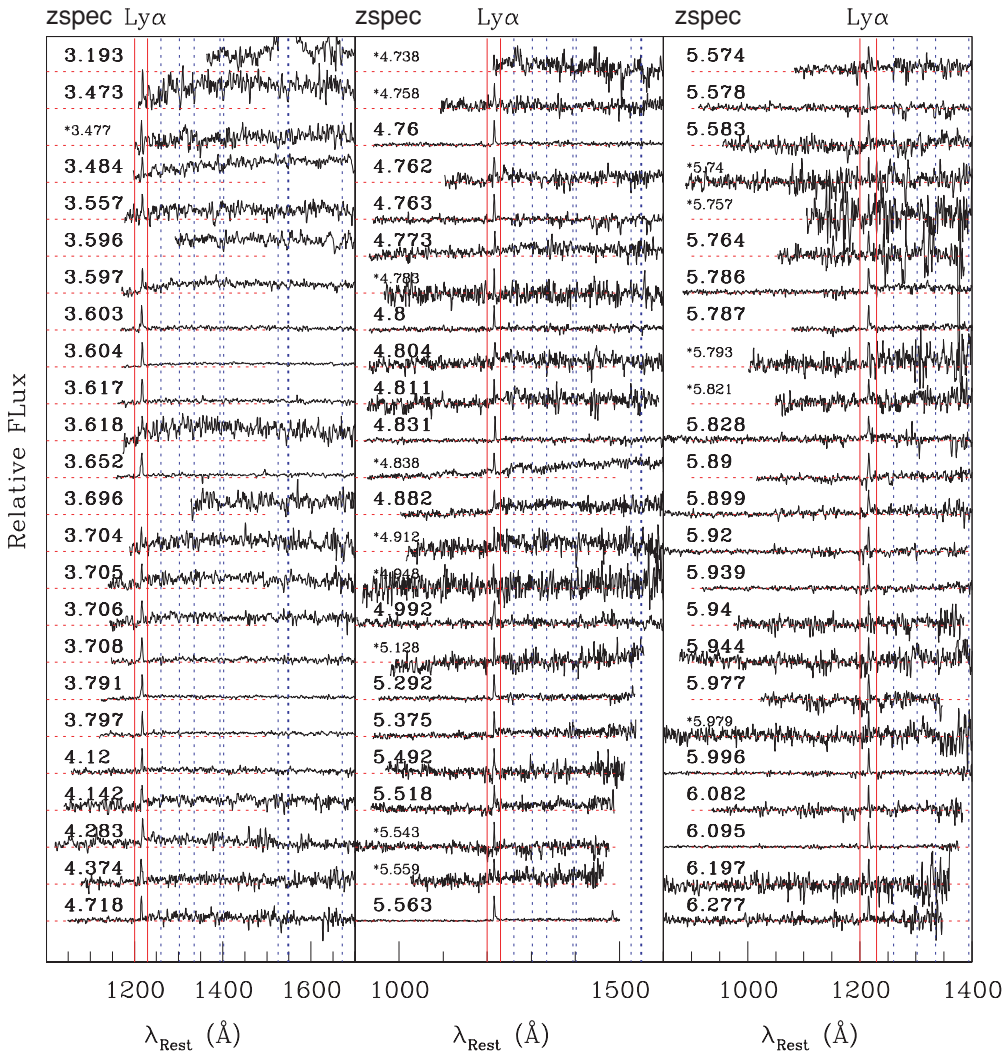

Figure 3. One-dimensional FORS2 rest-frame spectra of all emission line galaxies of the present sample. The redshift is indicated in the left side and the Lyα emission line is enclosed between the two vertical lines. Quality C (see the text) redshifts are marked with the $*$ symbol. Dotted vertical lines from left to right mark Si II 1260 Å, O I+Si II 1302 Å, C II 1335 Å, Si IV 1394,1403 Å, Si II 1527 Å, C IV 1548,1551 Å, and Al II 1670 Å in absorption, respectively.

(A color version of this figure is available in the online journal.)

observed with the low-dispersion ACS grism and show strong spectral breaks interpreted as due to the Lyα forest at $z \sim 5.9$ (Malhotra et al. 2005). These galaxies are present in our list with redshifts $z = 5.92$ and 5.95 (see Table 3). The source GDS J033234.55−274756.0, for which the FORS2 spectrum yielded an inconclusive redshift determination, is presented in Malhotra et al. (2005) at redshift $z = 6.1$.

Figure 2 shows the selection diagram for the i_{775}-band dropouts (dotted line). Galaxies confirmed in the redshift interval $5.6 < z < 6.5$ are marked with open squares. The majority of galaxies at $z > 5.6$ have (i_{775}−z_{850}) redder than 1.3, as per the adopted selection criteria. The confirmation of galaxies at redshift beyond five are almost exclusively due to the presence of a single emission line, identified as Lyα (see Section 5.4 for a dedicated discussion).

In the redshift interval $5.4 < z < 5.6$, the V_{606}- and i_{775}-band dropout selection criteria overlap. In this redshift range, five spectroscopically confirmed galaxies meet our V_{606}-band dropout selection criteria, while two meet the i_{775}-band dropout criteria. As discussed below, the presence of the Lyα emission line may play an important role in this respect.

Finally, as can be seen in Figures 1 and 2, of 114 high-redshift galaxies (109 targeted and five serendipitous), 12 are outside of the primary color-selection windows. Three of them are the above-mentioned "fillers," five are serendipitous sources discussed in Section 3, and nine are galaxies with colors close to the B_{435}-, V_{606}-, or i_{775}-band dropout selection windows (the mean "distance" in terms of color from the selection windows is $\Delta C \sim 0.04$). These galaxies were selected as B_{435}-, V_{606}-, or i_{775}-band dropouts from the previous (v1.0) ACS catalog, though in the current v2.0 catalog, they no longer meet the dropout selection criteria (see Table 5). We further note that seven out of these nine galaxies have been classified with QF = C. In particular, GDS J033233.52−275532.2, an i_{775}-band dropout at redshift $z = 5.74$ (QF = C), satisfied the i_{775}-band dropout selection criteria using the v1.0 catalog (in the v1.0 catalog, i_{775}−z_{850}=1.791), but not using the v2.0 catalog; it is no longer identified at S/N > 5 in the z_{850} band. A visual inspection of the z_{850} image suggests a faint source, as evident in Figure 7. However, further investigations will be needed to clarify this target; we do not include this source in the following analysis.

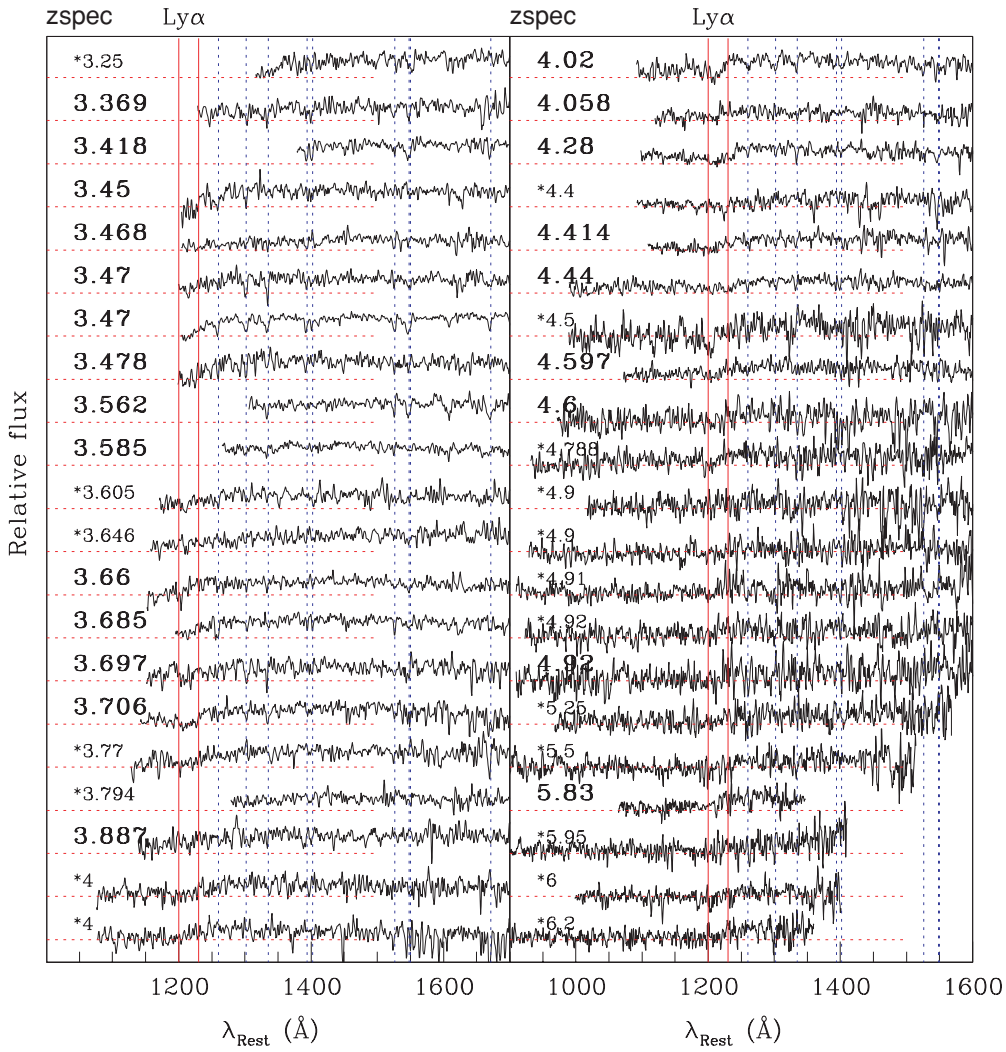

Figure 4. As in Figure 3, the one-dimensional FORS2 rest-frame spectra of all absorption line galaxies are shown. Beyond redshift ∼4.5, the spectra appear more noisy and the line identification is visually instable, the cross-correlation technique is particularly useful in these cases. The position of the Lyα line or the starting decrement by the IGM, is shown with solid vertical lines. Dotted vertical lines as in Figure 3.

(A color version of this figure is available in the online journal.)

5. COMPOSITE SPECTRA

We now describe, for each category of dropout, the general spectral properties observed. As in the case of LBGs at $z \sim 3$, and depending on the S/N, the most prominent rest-frame UV features observed in our samples are the H I Lyα line (seen in emission, absorption, or a combination of both), low-ionization, resonant interstellar metal lines such as Si II 1260 Å, O I + Si II 1302 Å, C II 1335 Å, Si II 1527 Å, Fe II 1608 Å and Al II 1670 Å, and high-ionization metal lines such as Si IV 1394,1403 Å and C IV 1548,1550 Å associated with P Cygni stellar wind features and ionized interstellar gas. In one case, [N IV]1485 Å emission has been detected together with Lyα in emission (GDS J033218.92−275302.7; Vanzella et al. 2006). As to be expected, the number of robustly identified lines decreases drastically with apparent magnitude over the range from $z_{850}\sim$ 24 to ∼26.5. At the faintest magnitudes, given our typical exposure times, continuum flux is at the limit of measurability (S/N ∼ 1 per resolution element) and therefore no absorption lines are reliably observed; the only observable feature for the faintest sources is Lyα emission.

5.1. B_{435}-Band Dropout Composite Spectra

Among 46 B_{435}-band dropouts with spectroscopic redshift at $z \approx 4$, 15 of them show Lyα in emission line (the "em." class), 21 have redshift identified by means of absorption lines only (the "abs." class)—typically Si II 1260.4 Å, C II 1335.1 Å, Si IV 1393.8,1402.8 Å, C IV 1548.2,1550.8 Å—and 10 sources show both emission and absorption features (the "comp." class). As mentioned above, two B_{435}-band dropouts have Lyα blueward of the observed spectral range, but this line was visible in second order at $\lambda > 10000$ Å; only absorption features were used to derive the redshifts for these sources. These two galaxies have not been used to make the composite spectra.

The composite spectra, normalized at 1450 Å, for emission line sources ("em." class), emission and absorption line sources ("comp." class) and absorption line sources ("abs." class) at $z \sim 3.8$ are shown in the left panel of Figure 8. The composite spectra include sources with QF = A, B, and C. A continuum break blueward of Lyα, due to the intergalactic medium (IGM), is clearly evident. Stellar and interstellar lines are also easily recognized.

Table 5
The Spectroscopic Sample of Galaxies Identified at Redshift Beyond 3 Serendipitously Discovered and/or Selected from the Previous Version (v1.0) of the ACS Catalogs and not Satisfying the v2.0 One (See the Text for Details)

GOODS ID	z	QF	Class	z_{850}	S/G	Comment
J033219.41−274728.4	3.250	C	abs.	24.65	0.33	serend. ($B-V=1.30$, $V-z=0.48$, v2.0)
J033234.40−274124.3	3.418	B	abs.	24.26	0.45	filler. ($B-V=1.42$, $V-z=0.55$, v2.0)
J033251.81−275236.5	3.468	A	abs.	25.03	0.04	filler. ($B-V=1.15$, $V-z=0.36$, v2.0)
J033206.53−274259.1	3.605	C	abs.	24.44	0.03	B_{435}-drop, from v1.0 ($B-V=1.59$, $V-z=0.52$, v2.0)
J033217.00−274113.7	4.414	B	abs.	25.09	0.02	V_{606}-drop, from v1.0 ($B-V=1.90$, $V-z=1.67$, v2.0)
J033218.27−274712.0	4.783	C	em.	27.60	0.90	serend. (Close to V_{606}-drop, pentagon in Figure 2).
J033243.16−275034.6[a]	4.838	C	em.	...	...	serend. (See Figure 2 of Vanzella et al. 2006)
J033228.94−274128.2[a]	4.882	B	em.	...	...	serend. (See Figure 13 of Vanzella et al. 2005)
J033222.71−275154.4	4.900	C	abs.	25.55	0.02	V_{606}-drop, from v1.0 ($V-i=1.76$, $i-z=0.30$, v2.0)
J033249.15−275022.5	4.910	C	abs.	25.54	0.99	V_{606}-drop, from v1.0 ($V-i=1.95$, $i-z=0.67$, v2.0)
J033211.71−274149.6	4.912	C	em.	25.36	0.05	V_{606}-drop, from v1.0 ($V-i=1.68$, $i-z=0.25$, v2.0)
J033222.89−274521.0[b]	5.128	C	em.	...	...	serend. (LAE?)
J033216.55−274103.2	5.250	C	abs.	25.69	0.00	i_{775}-drop, from v1.0 ($V-i=1.91$, $i-z=1.11$, v2.0)
J033228.55−275621.8	5.492	B	em.	27.45	0.96	i_{775}-drop, from v1.0 ($V-i=1.44$, $i-z=1.30$, v2.0)
J033239.82−275258.1	5.543	C	em.	26.53	0.15	filler, ($V-i=1.66$, $i-z=0.96$, v2.0)
J033233.52−275532.2[c]	5.740	C	em.	...	...	i_{775}-drop, from v1.0.
J033201.96−274406.5	5.821	C	em.	26.19	0.01	i_{775}-drop, from v1.0 ($V-i=1.49$, $i-z=1.20$, v2.0)

Notes.
[a] Sources not detected in the z_{850} band because blended to bright ones.
[b] Source not detected in the z_{850} band, only visible in the i_{775} band.
[c] Source originally detected in the v1.0 catalog, but not detected in the v2.0.

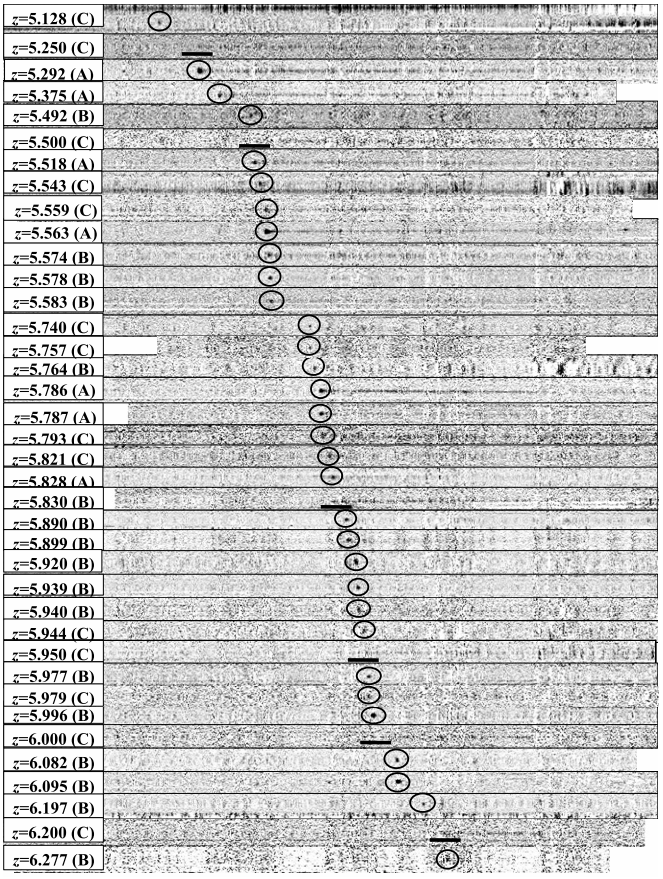

Figure 5. Two-dimensional FORS2 spectra of galaxies at redshift greater than 5. The redshift with its QF is indicated in the left side. The Lyα emission line is marked with a circle where present, otherwise a segment underline the possible continuum break.

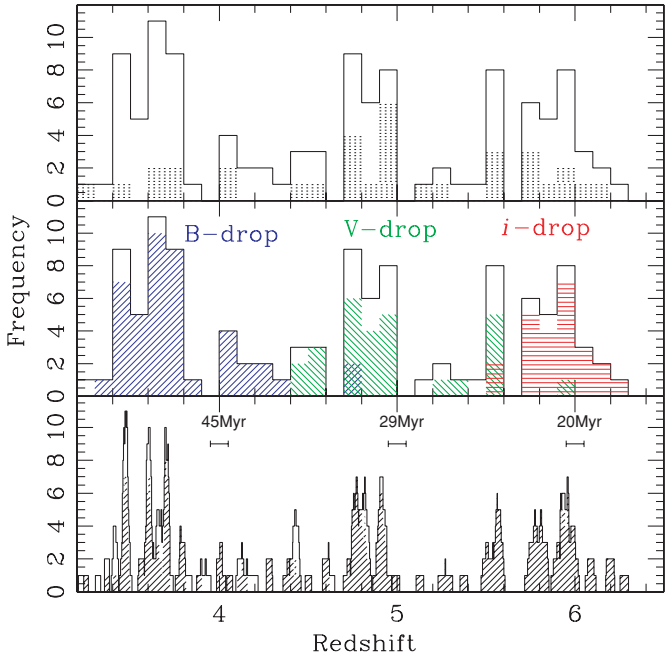

Figure 6. Redshift distribution of the LBGs spectroscopically confirmed in the GOODS-S field. Upper panel: the redshift distribution of all sources at redshift beyond 3 discovered during the FORS2 campaign is shown. The dotted area represents the sources with lower spectral quality (QF = C). Middle panel: the redshift distribution (continuum line) of the FORS2 sample with the highlighted categories B_{435}-, V_{606}-, and i_{775}-band dropouts (blue hatched "/" lines, green hatched "\" lines, and red horizontal lines, respectively) is shown. Bottom panel: the redshift distribution has been calculated counting the number of sources in a redshift bin of 0.1 and moving it with a step of 0.003 up to redshift 6.5 (the shaded region is the FORS2 spectroscopic sample and the continuum line histogram include the spectroscopic data from the literature (see the text)). The three segments indicate the interval of cosmic time for $dz = 0.1$ at the mean redshift of each category.

(A color version of this figure is available in the online journal.)

The absorption lines clearly differ between the "em.," "comp.," and "abs." classes. Figure 9 superposes the composite spectra of the B_{435}-band dropouts with and without the Lyα emission line ("em." and "abs."). Low-ionization interstellar absorption lines (ISLs) are more pronounced in the "abs." class composite spectrum; e.g., compare the O I, C II, and Fe II lines. Figure 9 also shows that the nonemitter population has a redder spectral slope, consistent with the previous work based solely on photometric data; e.g., Pentericci et al. (2007) find $\beta_{\rm phot}^{\rm em.} \sim -2.0 \pm 0.11$ and $\beta_{\rm phot}^{\rm abs.} \sim -1.7 \pm 0.13$, where $F(\lambda) \sim \lambda^{-\beta}$. A similar trend has also been noted by Shapley et al. (2003) from their sample of $z \sim 3$ LBGs. In particular, Shapley et al. (2003) find that the average extinction, $E(B-V)$, decreases as a function of increasing Lyα emission strength. The similar trends seen here at $z \sim 4$ suggest that the emission line B_{435}-dropout LBGs are, on average, less extincted than the absorption line B_{435}-dropout LBGs (see Pentericci et al. 2007).

5.2. V_{606}-Band Dropout Composite Spectra

As reported above, 32 V_{606}-band dropouts are at $z \approx 5$. As expected for the larger distance modulus and correspondingly fainter sample, the fraction of spectroscopically confirmed V_{606}-band dropouts with Lyα in emission is higher compared to the B_{435}-band dropout sample; 19 sources are in the "em." class and 13 show only absorption lines or a continuum break ("abs." class). The rest-frame composite spectra of emission and absorption galaxies with QF = A, B, and C are shown in the top left panel of Figure 8. Stellar and ISLs, as well as the strong continuum discontinuity at Lyα, are clearly observed in the composite spectra. The composite "em"-class spectrum looks quite similar to the B_{435}-band dropout composite "em" spectrum. For the "abs." class, the composite is dominated by low-quality (QF = C) spectra and only the strong Lyα forest break is apparent.

5.3. i_{775}-Band Dropout Composite Spectrum

The rest-frame composite spectrum of the emission line ("em." class) i_{775}-band dropouts is shown in Figure 10. Among the 28 i_{775}-band dropouts with spectroscopic redshift at $z \approx 6$, 22 sources show Lyα in emission (seven with QF = C).

Given the exposure times, these galaxies are generally too faint to measure a continuum (e.g., see Figure 3 or Figure 5) and only Lyα emission has been detected. As shown in Figure 11, this is particularly true for the fainter i_{775}-band dropouts. Nevertheless, the composite i_{775}-band dropout spectrum shows signal redward of the Lyα line, with tentative detection of the Si II 1260 Å and O I + Si II 1302 Å absorption lines despite the sky lines at these wavelengths being stronger and denser. At these high redshifts ($z \sim 5.9$), we find a very opaque IGM blueward of the redshifted Lyα line. Consistent with quasar results (e.g., Songaila 2004), the IGM transparency is estimated to be of the order of 1%.

5.4. Single-Line Redshift Identifications

For most of the $z \gtrsim 5$ LBGs in our sample, the redshift identifications are based on a single emission line—assumed to be redshifted Lyα—in an otherwise featureless and/or low-S/N spectrum. A question naturally arises: How robust are these identifications (e.g., Stern et al. 2000)? To be selected as dropouts, the broadband SED of these galaxies must satisfy the color-selection criteria, which require the signature of the Lyman limit and/or Lyα forest blanketing. The most plausible candidate for an alternate identification is [O II]3727 at $z \gtrsim 1.0$, though Hβ at $z \gtrsim 0.5$, [O III]5007 at $z \sim 0.5$, and Hα at $z \sim 0.1$ are also possible. Such possibilities, however, will generally be inconsistent with the broadband colors of the galaxies, since low-redshift solutions would be star-forming galaxies with relatively blue continua. This is illustrated in Figure 12, which plots the observed equivalent width versus the (i_{775}–z_{850}) color for [O II]-emitting galaxies at redshift $1 < z < 1.5$ and Lyα-emitting LBGs at redshift $z > 5$ (only galaxies with QF = A are plotted). Color and equivalent width do an effective job at separating the low-redshift, star-forming galaxies from their high-redshift counterparts, particularly for the i_{775}-band dropouts. A few V_{606}-band dropouts do overlap with the low-redshift galaxies, but are easily separated using (V_{606}–i_{775}) color, which is better suited for galaxies at $z \sim 5$.

The composite spectra of emission line V_{606}-band dropouts (Figure 8, right) and i_{775}-band dropouts (Figure 10) also provides evidence that most of the single-line Lyα identifications are correct. The $z \sim 5$ composite spectrum, which is a lower S/N version but otherwise virtually identical to the $z \sim 4$ composite spectrum (Figure 8, left), shows a number of absorption features that would not be observed due to dilution if most of the identifications were wrong. The $z \sim 6$ composite spectrum is similar, except that the lower S/N results in a lower S/N detection, or no detection at all, of absorption features. The continuum discontinuity across the Lyα, however, is clearly detected with a jump larger than one order of magnitude in the continuum flux density (in fact, the continuum blueward of the Lyα line is consistent with being zero). This is larger than other continuum discontinuities observed in distant galaxies (see Spinrad et al. 1998; Stern et al. 2000).

Finally, another discriminant between high-redshift and low-redshift single emission-line sources is provided by the line profile: high-redshift Lyα lines are asymmetric due to intervening HI absorption, while other lines will generally be symmetric. However, the low S/N, low spectral resolution ($R \sim 660$) reported here makes the detection of a clear asymmetry challenging in most individual spectra. In a few cases, however, an asymmetric profile has been detected in the brighter Lyα-emitting LBGs reported here.

6. OUTFLOWS AT $z \sim 4$ AND 5

Evidence of powerful winds in LBGs at $z \sim 3$ (Shapley et al. 2003) and in galaxies at $z \sim 2$ selected from UV colors (Shapley et al. 2005) has been inferred from the systematic redshift of the Lyα emission line and the blueshift of ISLs with respect to the systemic redshift of the galaxies, as traced by rest-frame optical nebular lines. In this scenario, the redshifted Lyα emission line forms in the receding part of a generally bipolar flow of gas, while the blueshifted interstellar lines originate in the part along the line of sight moving toward the observer.

6.1. Outflows in B_{435}-Band Dropouts ($z \sim 4$)

It is of interest to see if LBGs at $z \sim 4$ also show the same phenomenon, and compare its magnitude to that of the lower redshift galaxies, looking for evolutionary effects. Obtaining spectroscopic observations of the rest-frame optical nebular emission lines is not a trivial task. The [O II]3727, [O III]4959 and 5007 Å lines have been identified for only nine galaxies in our sample, as a part of the AMAZE project, aimed at estimating the mass–metallicity relation at high redshift (Maiolino et al.

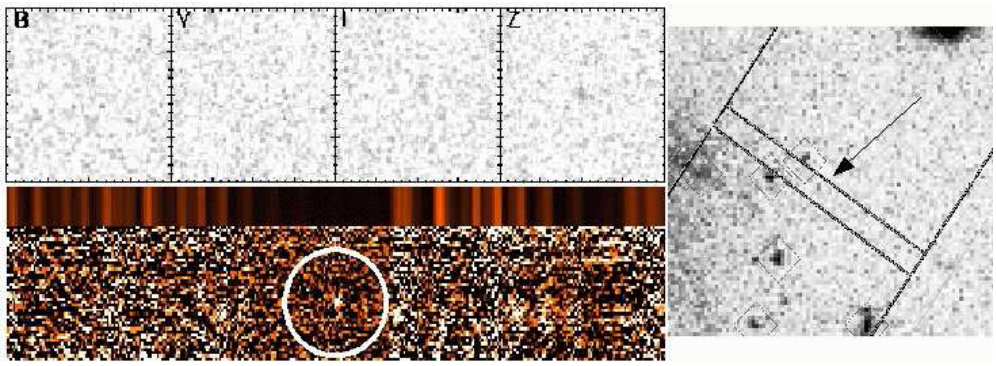

Figure 7. Cutouts, slit position on the sky and the two-dimensional extracted spectrum of the source GDS J033233.52−275532.2 (not detected in the v2.0 ACS catalog). Cutouts from left to right are B_{435}, V_{606}, i_{775}, and z_{850}, respectively, with 2 arcsec side box. On the right part of the figure the slit position is shown, and the faint source in the center, indicated by the arrow (in the images north is up and east on the left). On the bottom left, the two-dimensional spectrum is shown with the spot (marked with a circle) in the middle of the sky window at ∼8200 Å (see also Figure 15) and tentatively interpreted as Lyα emission, QF = C.

(A color version of this figure is available in the online journal.)

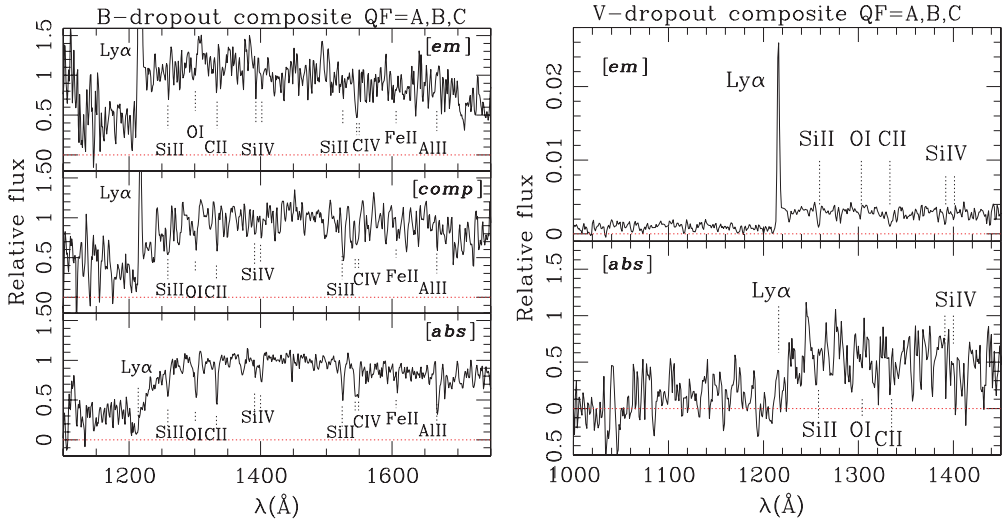

Figure 8. Left panel: the composite spectrum of B_{435}-band dropout galaxies with the Lyα emission line (top), Lyα emission and absorption features (middle) and only absorption features (bottom) is shown, respectively. The spectroscopic features are well recognized (for a detailed comparison between emitters (top) and absorbers (bottom), see Figure 9). Right panel: the same for the V_{606}-band dropout sources has been done for emitters (top) and absorbers (bottom). In the case of emitters, the absorption features are also clearly detected. In the case of absorbers, given the low-quality (QF = C) spectra and the small sample, only the Lyα forest break is apparent.

(A color version of this figure is available in the online journal.)

2008). In fact, these features become unreachable from the ground for redshift $\gtrsim$3.8 when the lines go beyond the K band. For such sources, information about the possible presence of winds is derived from the velocity differences between Lyα emission and ISLs.

The AMAZE project (Maiolino et al. 2008) has determined the redshift of nebular lines using the integral field spectrometer SINFONI at the VLT, adopting a spectral resolution $R = 1500$ in the spectral range 1.45–2.41 μm. For each source, the redshift derived from [O III]4959,5007 Å and [O II]3727 agree within $|\Delta z| \sim 10^{-3}$. We have calculated "nebular redshifts" for each galaxy by averaging these three lines. The redshift of the interstellar medium has been derived from the low-ionization ISLs (e.g., Si II 1260 Å, O I+Si II 1302 Å, C II 1335 Å, and Si II 1527 Å), and the redshift of the hydrogen gas is estimated from the Lyα line.

We then compare the various redshift estimates arising from the different physical regions within the LBGs, i.e., the velocities $V_{\mathrm{Ly}\alpha}$, V_{ISL}, and V_{nebular}. We find that

1. the relative median velocity $\langle V_{\mathrm{Ly}\alpha} - V_{\mathrm{ISL}} \rangle$ observed between the Lyα emission lines and the ISLs is $+370^{+270}_{-116}$ km s^{-1} (derived from 16 galaxies at an average redshift of 3.70 ± 0.2). The Lyα emission is always redshifted relative to the interstellar lines. Adopting the model of Verhamme et al. (2006), the velocity V_{exp} of the expanding neutral hydrogen shell is of the order of 120–180 km s^{-1};
2. the relative median velocity $\langle V_{\mathrm{Ly}\alpha} - V_{\mathrm{nebular}} \rangle$ between the Lyα emission line and the nebular lines is $+161 \pm 80$ km s^{-1} (derived from four galaxies at $z \sim 3.65$);
3. the relative median velocity $\langle V_{\mathrm{ISL}} - V_{\mathrm{nebular}} \rangle$ between the ISLs and the redshift of the nebular lines is -165^{+170}_{-194} km s^{-1} (derived from nine galaxies at $z \sim 3.7$).

The galaxy GDS J033217.22−274754.4, with its peculiar, double-peaked Lyα profile is already been discussed in detail in Vanzella et al. (2008).

Figure 13 shows the histogram of $(V_{\mathrm{Ly}\alpha} - V_{\mathrm{ISL}})$ for the 16 galaxies from the B_{435}-band dropout sample for which this

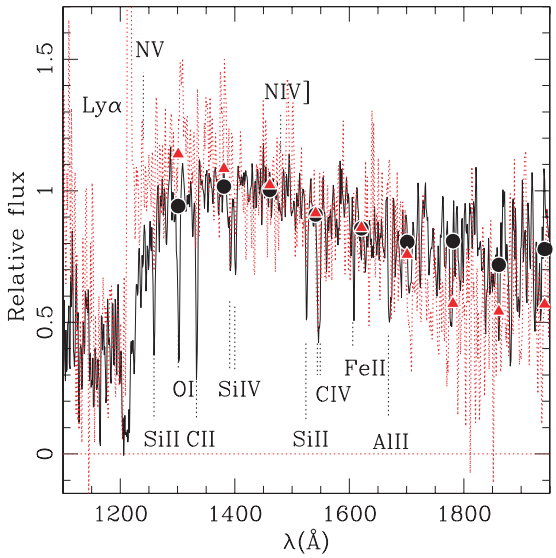

Figure 9. Comparison between composite spectra normalized at 1450 Å of the B_{435}-band dropout galaxies with and without the Lyα emission line (emitters and absorbers). The circles are the median values calculated in bins of 100 Å of the absorbed stacked spectrum, while the triangles are those of the emission stacked spectrum. The bluer spectral slope of the "emitter" population is evident and in general the absorption lines of the emission stacked spectrum are weaker than the absorbed spectrum.

(A color version of this figure is available in the online journal.)

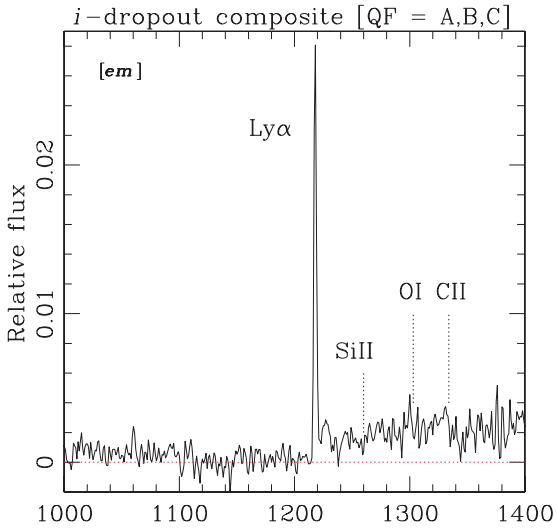

Figure 10. Composite spectrum of i_{775}-band dropout emission line galaxies. A faint signal reward the Lyα line is clear, and there is a tentative detection of absorption lines, whose expected position is probably disturbed by the sky line residuals (especially at λ beyond 1340 Å). The shape of the spectrum shows the attenuation of the IGM blueward the Lyα line.

measurement has been possible. The histogram does not include quality QF = C spectra. In all cases, the redshift of the Lyα is measured by fitting a Gaussian profile to the line,[14] while the redshift of the ISLs is derived cross correlating the individual spectra with templates (namely, the lensed galaxy cB58 and the composite spectrum without Lyα emission from Shapley et al. 2003), after excluding the Lyα line from the analysis. The typical

[14] As simulated in Verhamme et al. (2008), the effect of the spectral resolution on the measurement of the Lyα barycenter is more important for galaxies with broad Lyα absorption. In the case of emission, like the objects reported here, this is not the case—the lines are narrow. Because the lines are nearly unresolved, asymmetry has little effect on the measured central wavelength.

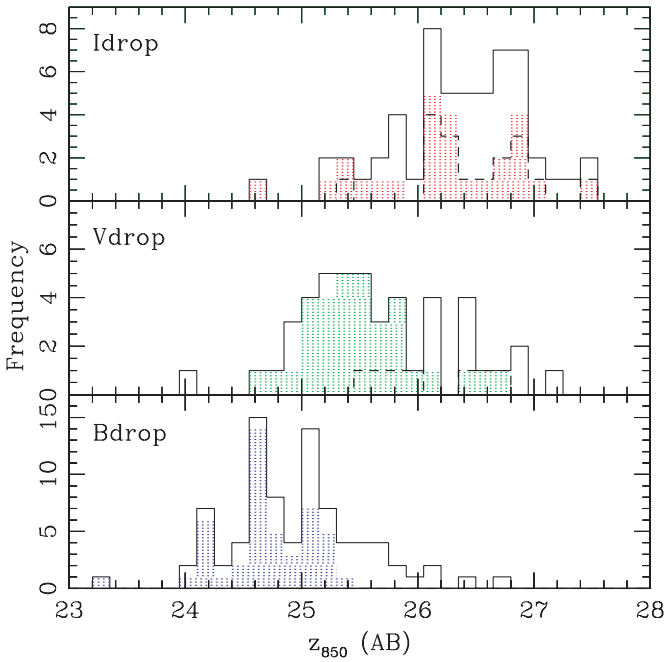

Figure 11. z_{850}-magnitude distribution of the three B_{435}-, V_{606}-, and i_{775}-band dropout samples. Solid line histograms show the magnitude of all targets observed, dotted regions show the sources with a redshift measure, and dashed histogram outlines the sources for which a single emission line (without continuum) has been observed and used in the redshift measurement (Lyα). It is evident in the single-line detection for the fainter galaxies (z_{850} magnitude beyond ∼26). For the B_{435}-band dropout sample, all galaxies show the continuum.

(A color version of this figure is available in the online journal.)

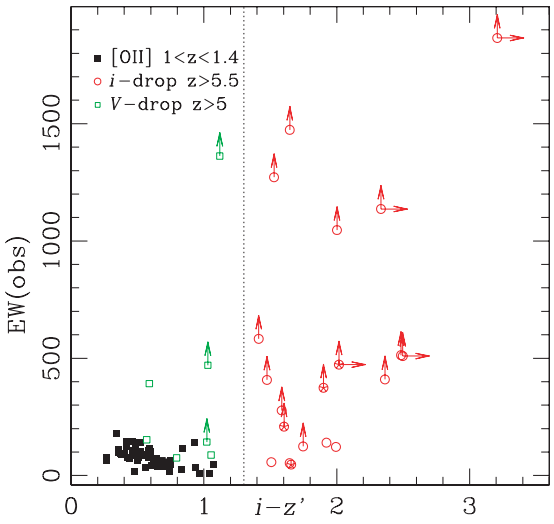

Figure 12. Comparison of the observed equivalent widths of Lyα and [O II]3727 lines for the samples of galaxies at redshift >5 and redshift ∼1–1.4, respectively. This is a further indication of the high-redshift nature of the single line detected for dropout galaxies. Three out of four V_{606}-band dropouts relatively close to the zone of [O II]3727 galaxies have been confirmed with QF = A, both the Lyα line and the continuum are evident in the spectra. One is a QF = B and the equivalent widths of Lyα is a lower limit (see the text for a detailed discussion).

(A color version of this figure is available in the online journal.)

redshift error is $\Delta z \sim 0.001$ (Vanzella et al. 2008, derived from multiple, independent observations) and translates into a final error on the velocity difference $\Delta(V_{\mathrm{Ly}\alpha} - V_{\mathrm{ISL}}) \sim 64\,\mathrm{km\,s^{-1}}$ at $z \sim 3.7$. Figure 13 shows that the Lyα line is systematically redshifted relative to the ISLs and a few galaxies have velocity differences in excess of 600 km s^{-1}.

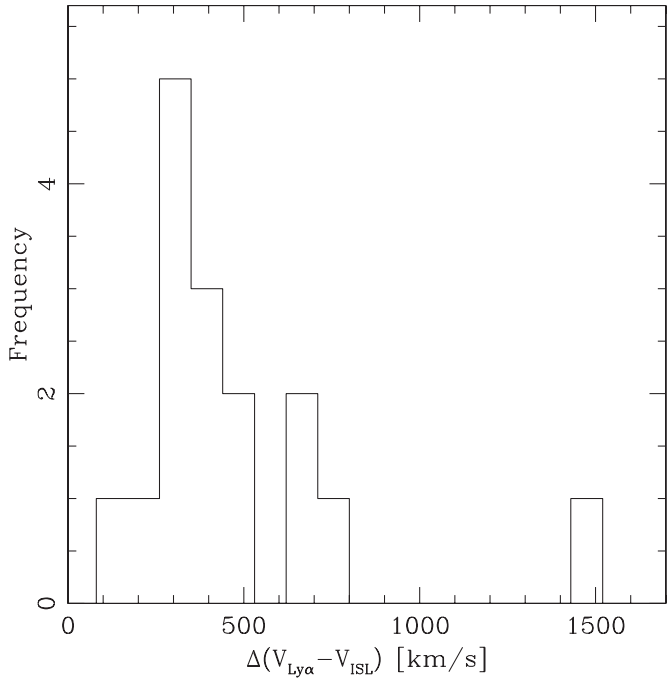

Figure 13. Velocity differences between the Lyα line and the ISLs ($V_{\mathrm{Ly}\alpha} - V_{\mathrm{ISL}}$) for 16 galaxies of the B_{435}-band dropout sample. The median of the distribution is 370^{+270}_{-116} km s^{-1} (see the text for details).

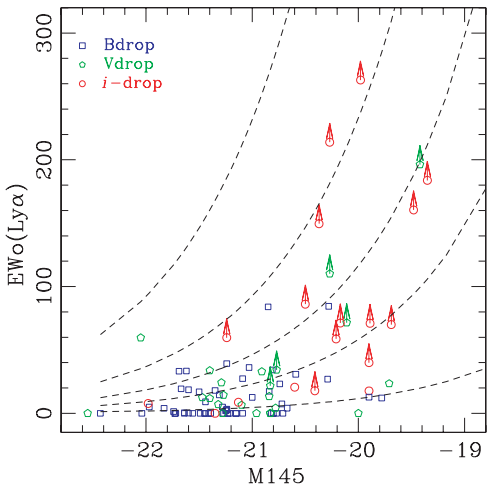

Figure 14. Rest-frame Lyα equivalent width as a function of the UV luminosity (M_{145}, absolute magnitude at 1450 Å) for all the galaxies at redshift beyond 3.1. Dashed curves represent the equivalent widths at fixed Lyα luminosity, from top to bottom 5, 2, 1, 0.5, and 0.1 $\times$ 10^{43} erg s^{-1}, respectively. There is a clear trend for the Lyα equivalent width to increase, on average and in its maximum value, for fainter objects.

(A color version of this figure is available in the online journal.)

Though derived from relatively small samples, these numbers are similar to LBGs at $z \sim 3$ (Shapley et al. 2003; Adelberger et al. 2003). In particular, Figure 11 of Shapley et al. (2003) shows that with increasing Lyα emission strength, the kinematic offset implied by the relative redshifts of Lyα emission and low-ionization ISLs decreases monotonically from $\langle V_{\mathrm{Ly}\alpha} - V_{\mathrm{ISL}} \rangle = 800\,\mathrm{km\,s^{-1}}$ to $\langle V_{\mathrm{Ly}\alpha} - V_{\mathrm{ISL}} \rangle = 480\,\mathrm{km\,s^{-1}}$. If we assume this trend remains true at $z \sim 3.7$ and consider the mean rest-frame Lyα equivalent width of our sample (20 Å), the comparison is even more consistent with the results at $z \sim 3$. We also note that the $\langle V_{\mathrm{ISL}} - V_{\mathrm{nebular}} \rangle = -150$ km s^{-1} derived by Adelberger et al. (2003) is similar to the value derived here at slightly higher redshift, -165 km s^{-1}.

6.2. *Outflows in V_{606}-Band Dropouts and at Redshifts Beyond 5*

In the case of V_{606} dropouts ($z \sim 5$), the mean velocity difference $\langle V_{\mathrm{Ly}\alpha} - V_{\mathrm{ISL}} \rangle$ is more difficult to estimate for individual galaxies because the S/N is generally lower, due to both the faintness of the targets and to the UV absorption features entering a spectral region affected by strong sky emission lines at $z \gtrsim 4.5$. For this reason, we have resorted to estimating $\langle V_{\mathrm{Ly}\alpha} - V_{\mathrm{ISL}} \rangle$ from the composite spectrum. All V_{606}-band dropouts with Lyα in emission have been co-added, registering their redshift with respect to their Lyα lines. This procedure will lead to a slight smoothing of the interstellar lines and thus a larger uncertainty. Nevertheless, an absorption signal remains clearly detected in the composite spectrum.

The UV absorption features Si II 1260.4 Å, C II 1335.1 Å, and Si IV 1393.8,1402.8 Å (see Figure 8) show an average blueshift of $\sim -450\,\mathrm{km\,s^{-1}}$ with respect to the Lyα line, similar to the B_{435}-dropout results. With the aim of extending this measurement to yet higher redshift, we have selected a subsample of eight LBGs with detected continuum at $z > 5$ from the V_{606}- and i_{775}-band dropout samples, at an average redshift of 5.6 and z_{850} magnitude 25.6 (three i_{775}-band dropouts and five V_{606}-band dropouts; QF = C LBGs have not been considered). Similar to the sample of pure V_{606}-band dropouts, the composite spectrum shows a velocity offset of $(V_{\mathrm{Ly}\alpha} - V_{\mathrm{ISL}}) \sim +500\,\mathrm{km\,s^{-1}}$.

In order to check if the above estimations give realistic measurements of the offset, we have re-calculated ($V_{\mathrm{Ly}\alpha} - V_{\mathrm{ISL}}$) from the B_{435}-band dropout composite spectrum. We find $(V_{\mathrm{Ly}\alpha} - V_{\mathrm{ISL}}) \sim +490\,\mathrm{km\,s^{-1}}$. Though a bit higher, this value is consistent with the number derived from individual measurements.

This analysis performed therefore supports the interpretation that outflows at $z \sim 4$ and 5 are present and similar to those seen at lower redshifts ($z \sim 2$–3).

7. Lyα EQUIVALENT WIDTH AND THE UV LUMINOSITY

For all galaxies with Lyα in emission, we have estimated the rest-frame equivalent width of the line. In the critical cases where this line is the only feature detected in the spectrum, the continuum has been estimated from the available photometry assuming a flat spectrum with spectral index $\beta = -2.0$ ($f_\lambda \propto \lambda^\beta$). Depending on the redshift, the i_{775} ($z \leqslant 4.65$), z_{850} ($4.65 < z \leqslant 5.7$), or Js ($z > 5.7$) magnitudes have been used to determine the continuum level. In the highest redshift case, we use Js magnitudes (the Js filter has a central wavelength of 1.24 μm and width of 0.16 μm, it allows an accurate photometry) from the GOODS-MUSIC catalog (Grazian et al. 2006), or the NIC3 F110W band magnitude (Thompson et al. 2006) for sources in the HUDF. If the magnitude is a lower limit, the resulting equivalent width is a lower limit (indicated by an arrow in the figures). The absolute M_{145} magnitude has been derived from the z_{850} band, assuming a template (drawn from SB99; Leitherer et al. 1999) of a star-forming galaxy with spectral index $\beta \sim -2.0$.

Figure 14 shows the distribution of the rest-frame equivalent widths versus the absolute magnitude calculated at 1450 Å for all sources in the sample. A cosmic time between 0.9 and 1.6 Gyr after the big bang is covered (B_{435}-, V_{606}-, and i_{775}-band dropouts are marked with different symbols). At fainter luminosities

($M_{145} > -21$), the estimated equivalent widths span a wide range of values, from a few Angstroms up to 300 Å. There is a natural observational bias that the redshift of the faintest, high-redshift galaxies can only be measured if they contain a strong, high equivalent width Lyα line. However, there is no such bias against high equivalent width for *brighter* galaxies, but these are not observed. This absence of large equivalent widths of Lyα lines at bright luminosities has already been noted by several groups studying samples of Lyα emitters (LAEs) and LBGs at redshift between 3 and 6 (e.g., Shapley et al. 2003; Ando et al. 2006, 2007; Tapken et al. 2007; Verhamme et al. 2008).

The equivalent width of the Lyα line (or the escape fraction of the Lyα photons) is related to the velocity expansion $V_{\rm exp}$ of the medium, the column density of the neutral gas $N_{\rm HI}$, the dust extinction $E(B-V)$, and the geometry of the media (clumpy or continuum geometry). A possible scenario is that the brighter galaxies are experiencing (or have already experienced) a higher burst of star formation and supernovae explosions with an associated production of dust. Thus, the more luminous galaxies would be dustier and more metal-rich, have correspondingly more efficient Lyα absorption, and thus exhibit lower observed Lyα equivalent widths. Larger equivalent widths are expected for objects dominated by younger ($\gtrsim$10–40 Myr) stellar populations; lower equivalent widths are expected in dusty and/or post-starburst galaxies (e.g., Schaerer & Verhamme 2008). This hypothesis implies that brighter LBGs would be dustier, more chemically enriched, and show lower equivalent widths (Lyα). One would expect that ultimately the main underlying parameter governing the trends with UV magnitude might be the galaxy mass.

Finally, we note that fixing the redshift (i.e., the dropout flavor) in Figure 14, the deficiency of strong lines at bright UV magnitudes remains, though better statistics are clearly needed, particularly at the faint end of the redshift distributions.

On the other side of the distribution, the presence of large Lyα equivalent widths for faint sources may be a combination of selection effects and intrinsic properties of these galaxies.

1. *Observational bias:*
   (a) *Spectroscopy.* Obviously, from the spectroscopic point of view, faint galaxies (mainly i_{775}-band dropouts) are confirmed; thanks to the presence of an Lyα emission line that can be observed also in the middle of the sky emission (see Figure 15). In the current spectroscopic sample, fainter galaxies tend to be at higher redshifts. Figure 16 shows the behavior of Lyα luminosity versus redshift. There is an indication that the fraction of stronger lines increases with redshift (also noted by Frye et al. 2002).
   (b) *Photometry.* Strong Lyα emission also affects photometric color selection—in particular, for i_{775}-band dropouts which rely on a single color (i.e., $i_{775}-z_{850} > 1.3$). At $z > 5$, the contribution of Lyα emission to the $(i_{775}-z_{850})$ color range up to $\approx$0.5 (0.8) mag for Lyα rest-frame equivalent widths of 100 Å (150Å), consistent with the measurements in our spectroscopic sample (see Figure 17). The $(i_{775}-z_{850})$ color is increased or decreased depending on the strength of the line and the redshift of the source. Two clear examples (marked with star symbols in Figure 17) are as follows.
      (i) GDS J033218.92−275302.7 ($z = 5.563$) shows an Lyα emission line with rest-frame equivalent width of ∼60 Å falling within the i_{775} band. This has the effect of reducing the apparent $i_{775}-z_{850}$ color by 0.59 mag. This galaxy has been selected as a V_{606}-band dropout and is also discussed as a candidate "Balmer Break galaxy" based on its bright IRAC flux and apparent "break" in the $K-3.6$ μm colors (Wiklind et al. 2008).
      (ii) GDS J033223.84−275511.6 ($z = 6.095$) shows an Lyα emission line with no continuum detected in 80 ks of spectroscopy. The rest-frame equivalent width is $\gtrsim$250 Å, and the measured $(i_{775}-z_{850})$ color is a lower limit ($(i_{775}-z_{850}) > 3.2$). In this case, the z_{850} apparent magnitude (and the $(i_{775}-z_{850})$ color) is increased by the line.
   In order to explore such effects as a function of redshift, Lyα equivalent width, and z_{850} magnitude, we have calculated various color tracks as shown in Figure 18. We find that, when the Lyα line enters the z_{850} band ($z > 5.6$) and leaves the i_{775} band ($z > 5.9$), depending on the equivalent width, it favors the i_{775}-band dropout selection criteria. For fainter sources ($z_{850} > 26.5$), only the emitters tend to survive.
2. *Intrinsic effects.* The large spread in Lyα equivalent widths at faint magnitudes ($M_{145} \lesssim -21$) observed by numerous authors may also be due to a relatively small amount of dust, which would not filter out the stronger Lyα lines, and to a larger variety of star formation histories and timescales—i.e., an enhanced role of "stochastic star formation events." Such a scenario is most likely to have a strong effect for galaxies of smaller absolute scale (either mass or total star formation rate; Verhamme et al. 2008).

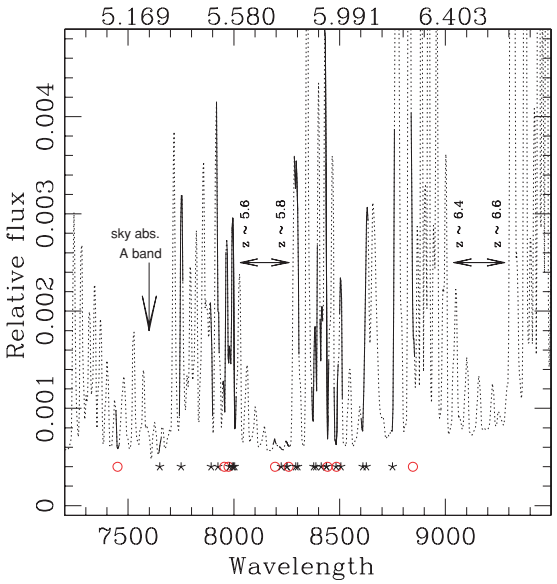

Figure 15. The positions of the Lyα lines (solid line) for galaxies at redshift beyond 5 are marked on the sky spectrum (dotted line). Stars and open circles denote the redshift of the Lyα position of galaxies with QF = A, B, and C, respectively. The lines have been detected sparsely in the forest of the sky emission. The sky-free windows at redshifts ∼5.7 and ∼6.5 are also shown.
(A color version of this figure is available in the online journal.)

We further note that at $z \gtrsim 6$ the age of the universe is of the order of the duration of the LBG phase (∼0.5–1 Gyr; Shapley et al. 2001; Papovich et al. 2001; Lee et al. 2008).

Assuming an initial interval of time ($\Delta t_{{\rm Ly}\alpha}$) in which the LBG is active as an LAE (i.e., shows conspicuous Lyα emission, with rest-frame equivalent width greater than 100 Å), whose

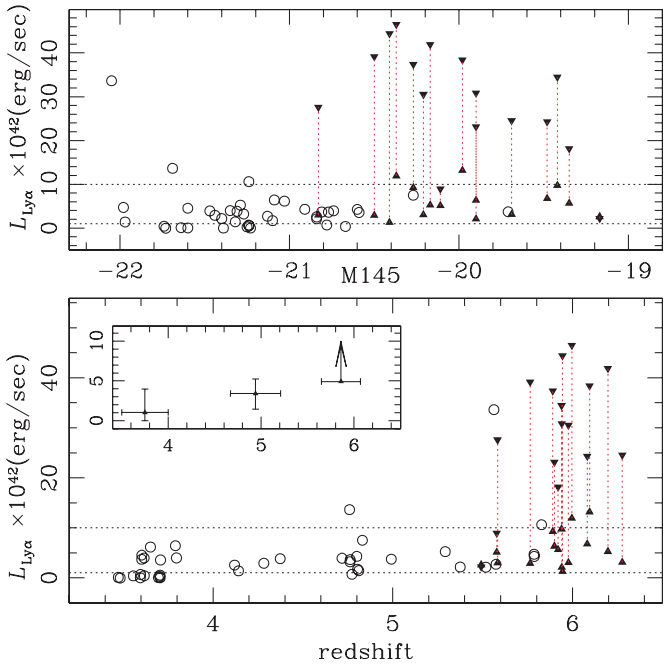

Figure 16. Top: the Lyα luminosity as a function of the M_{145} magnitude. Bottom: Lyα luminosity as a function of the redshift. In the inner box, the same figure is shown but the medians have been calculated at the average values of the three categories: B_{435}-, V_{606}-, and i_{775}-band dropouts. For both panels, the filled triangles connected by a dotted line represent the lower limit and upper limit to the Lyα luminosity for galaxies without continuum detected in the spectra. The lower limit is simply the integral of the Lyα line, while the upper limit is calculated assuming that the entire z_{850} flux is due to the line. Dotted horizontal lines mark the 10^{42} and 10^{43} erg s^{-1} luminosity, respectively.

(A color version of this figure is available in the online journal.)

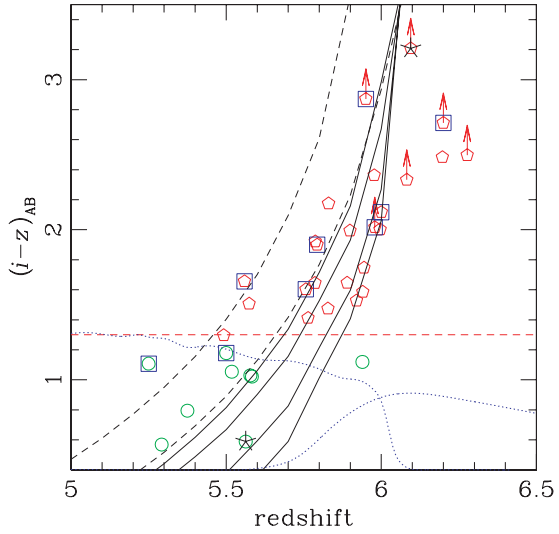

Figure 17. Color–redshift diagram of the spectroscopic sample at redshift beyond 5. The six curves show the predicted (i_{775}–z_{850}) color for different templates spectra. The templates have been built combining synthetic spectra (drawn from SB99) with different Lyα equivalent widths. The two dashed lines from left to right have stellar populations of 10^8 and 10^7 yr, respectively, and no emission Lyα is present. The four solid lines from left to right are color tracks assuming a fixed template of 10^7 yr (from SB99) with the addition of Lyα emission line with rest-frame equivalent widths of 30, 50, 100, and 150 Å, respectively. The attenuation of the IGM has been implemented adopting the prescription of Madau (1995). Open squares are sources with QF = C, pentagons and open circles are i_{775}- and V_{606}-band dropouts, respectively. The dotted curves are the shapes of the filters i_{775} and z_{850}, and show at which redshift the Lyα line enter and leave them. The two stars mark two peculiar galaxies (see the text).

(A color version of this figure is available in the online journal.)

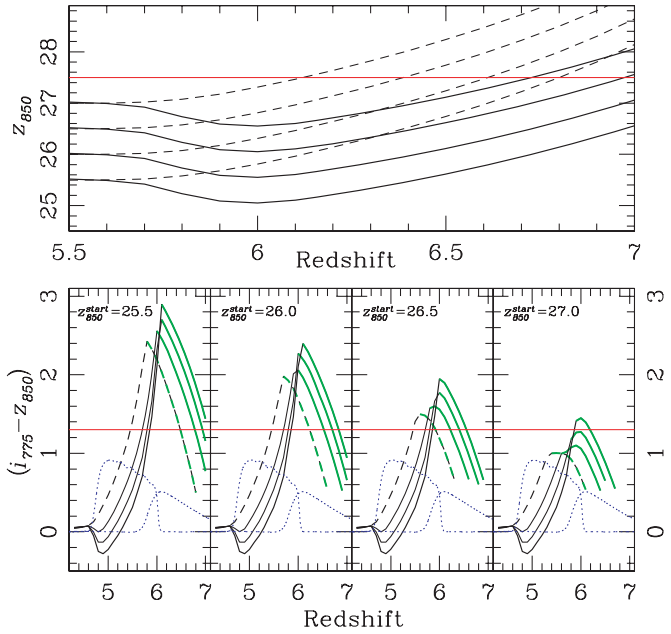

Figure 18. Top: pure luminosity–redshift dimming of the z_{850} apparent magnitude calculated so that at redshift 5.6 (Lyα just blueward the z_{850} band) it is 25.5, 26, 26.5, 27 from bottom to top curves. Solid line is the magnitude track of an SB99 template (with age of the stellar population of 100 Myr) with Lyα emission inserted with the rest-frame equivalent width of 150 Å, the dashed lines without Lyα line inserted. Bottom: the (i_{775}–z_{850}) color as a function of the redshift, the z_{850} magnitude and the Lyα rest-frame equivalent width: dashed lines correspond to an equivalent width of 0 Å, solid lines from left to right correspond to 50, 100, and 150 Å, respectively. The thick green lines represent the regions where the color becomes a lower limit (assuming the limit of the GOODS Survey in the i_{775} band to be 28.0 at 2σ). All lines have been plotted with the condition $z_{850} < 27.5$. The red horizontal line is the color cut adopted for the selection of $z \sim 6$ galaxies. The shapes of the i_{775} and z_{850} filters redshifted to the Lyα position are also reported, blue dotted lines (Lyα line enter the z_{850} band at redshift ~5.6 and leaves the i_{775} band at redshift ~5.9). It can be seen that fainter galaxies at $z > 5.6$ tend to be selected with a strong Lyα line.

(A color version of this figure is available in the online journal.)

duration should be of the order of 100–300 Myr (e.g., Mori & Umemura 2006; Verhamme et al. 2008), the probability to observe an LBG in the LAE phase should increase with redshift when observing galaxies in a universe younger than ~0.5–1 Gyr (roughly, the fraction of emitters vs. nonemitters is proportional to $\Delta t_{Ly\alpha}/\tau(z)$). Future surveys of LBGs at redshift beyond seven should show this trend even more clearly (albeit subject to the observational selection effects discussed above).

8. CORRELATION WITH MORPHOLOGICAL PROPERTIES

We have derived basic morphological parameters for the galaxies in our spectroscopic samples from the ACS z_{850}-band image. With an effective wavelength $\lambda_{eff} \approx 9100$ Å (for a typical LBG UV spectrum), the z_{850} filter probes the rest-frame far-UV emission of B_{435}-dropout galaxies at $\lambda_0 \approx 2000$ Å. In general, it is difficult to interpret the results of analyses of the UV morphologies of high-redshift galaxies in terms of the evolution of traditional Hubble types, in part because these are mostly known at optical rest-frame wavelengths (see Giavalisco et al. 1996), and also because it is not obvious what is the typical morphology of the present-day spectral types that are most similar to the $z \sim 4$ LBGs (Overzier et al. 2008).

Table 6
Basic Morphological Parameters for B_{435}-Band Dropout Galaxies, Dividing Between Emitters and Nonemitters

	EM. ($\langle z\rangle = 3.757$)	ABS. ($\langle z\rangle = 3.735$)
a	4.54 ± 1.03	6.51 ± 2.18
h.l.r.	5.38 ± 1.65	7.49 ± 2.85
Area	305 ± 117	438 ± 172
FWHM	10.38 ± 4.06	20.01 ± 11.97
Gini	$0.41^{+0.11}_{-0.06}$	$0.26^{+0.18}_{-0.10}$

Notes. For the first four rows, the values are reported in pixels, while the Gini coefficient measure the nucleation of the source light (see the text for details).

We have measured parametric and nonparametric morphological indicators separately for the two subsamples of "emitters" and "absorbers" in the $z \sim 4$ primary sample. The basic morphological parameters have been drawn from the v2.0 ACS catalogs, direct outputs of the SExtractor algorithm during the segmentation process in the z_{850} band, and are summarized in Table 6 with their average values and 1σ standard deviations. Tabulated quantities are the major semiaxis (a), half-light radius (h.l.r.), isophotal area (AREAF), and FWHM. As shown in Table 6, LBGs with Lyα in emission have more compact morphologies relative to those with rest-frame UV features observed in absorption. In detail, the physical sizes at the h.l.r. for emitters and absorbers are on average 1.1 and 1.6 kpc, respectively.

To further investigate the correlation between morphology and Lyα properties, we have computed the Gini coefficient for our sample. We have utilized the formulation described in Abraham et al. (2003, their Equation (3)). The Gini coefficient provides a measure of the degree of central concentration of the source. Values range between 0 (uniform surface brightness) and 1 (highly nucleated). Lotz et al. (2006), Ravindranath et al. (2006) and, more recently, Lisker (2008), have analyzed the stability of the Gini coefficient, based on a comparison of *HST*/ACS imaging data from the GOODS and UDF Surveys. They find the Gini coefficient depends strongly on the S/N and at all S/N levels, the Gini coefficient shows a strong dependence on the choice of aperture within which it is measured. This complicates comparisons of Gini parameters derived in different studies. However, relative values from measurements done the same way within a given data set should be meaningful. In the present case, we restrict the analysis for the brighter B_{435}-dropout sample and assume that systematics are similar for both emitter- and absorber-class LBGs. The pixels of each source used in the calculation are those with flux above $F \times 1\sigma$ percentile of the median background. Adopting $F = 2$ and the z_{850} band ($F = 2$, z_{850} band), we find that the "em." and "abs." classes have $G_{\rm em} = 0.41^{+0.11}_{-0.06}$ and $G_{\rm abs} = 0.26^{+0.18}_{-0.10}$, respectively. With ($F = 3$, z_{850} band), the values are $G_{\rm em} = 0.31^{+0.09}_{-0.09}$ and $G_{\rm abs} = 0.18^{+0.11}_{-0.08}$. The same calculation performed in the i_{775} band, produces the following median values: $G_{\rm em} = 0.49^{+0.10}_{-0.16}$, $G_{\rm abs} = 0.26^{+0.14}_{-0.09}$ ($F = 3$, i_{775} band) and $G_{\rm em} = 0.61^{+0.11}_{-0.15}$, $G_{\rm abs} = 0.35^{+0.19}_{-0.14}$ ($F = 2$, i_{775} band).

These calculations show that the two LBG spectroscopic classes have different average morphologies, with emitters intrinsically more nucleated than the absorbers. This distinction seems to increase with greater Lyα equivalent width. The behavior is shown in Figure 19 (middle panel, $F = 2$, z_{850} band), where the Gini coefficient is plotted versus the Lyα equivalent width. Though this result is, on average, in qualitative agreement with the observations at $z \sim 2$ and 3 by Law et al. (2007), we note that cases of nucleated absorbers and "fuzzier" emitters are also present. Larger galaxy samples at these redshifts are needed in order to put this result on a firmer statistical footing.

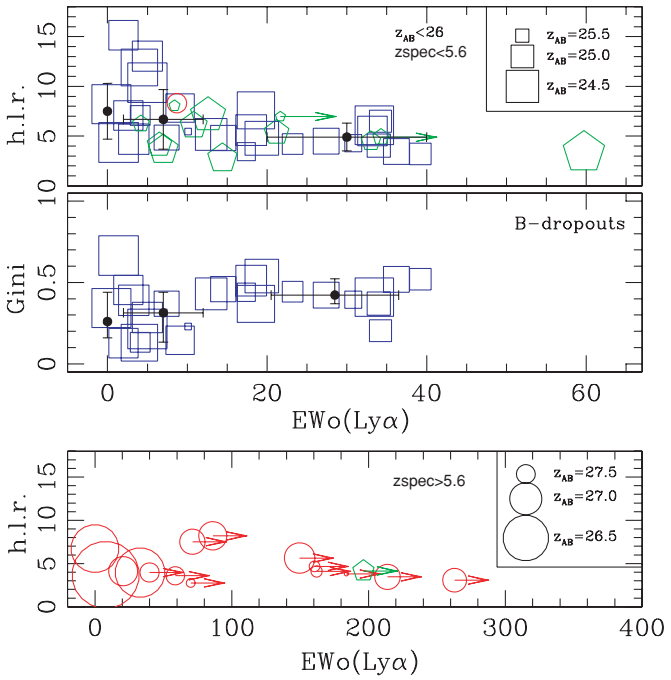

Figure 19. Top: h.l.r. vs. Lyα equivalent width. Squares, pentagons, and open circles mark B_{435}, V_{606}, and i_{775} dropouts, respectively. The size of the symbols scale with apparent z_{850} magnitude. Only sources with z_{850} below 26 and redshift below 5.6 (~0.8 Gyr of the cosmic time is probed in the redshift range 3.5–5.6) are plotted (see the text for details). For comparison, the filled circle at 0 Å is the average h.l.r. for galaxies without Lyα emission line. The other two filled circles are the averages for sources in the bin 0–20 Å and beyond 20 Å. There is an apparent behavior such that larger Lyα equivalent widths correspond to smaller galaxies. Middle: Gini coefficient vs. Lyα equivalent width only for the B_{435}-dropout sample. The filled circle at 0 Å is the average of the absorbers, the other two filled circles are the averages of the Gini parameter in the bin 0–20 Å and beyond 20 Å. Sources with larger Lyα equivalent widths seem to be more nucleated. Bottom: same as the top panel, but for galaxies with redshift beyond 5.6 (mainly i_{775} dropouts). In all panels, no QF = C have been considered.
(A color version of this figure is available in the online journal.)

As shown in Figure 19 (top panel), there also seems to be an inverse correlation between Lyα emission equivalent width and galaxy size, namely galaxies with larger equivalent widths are smaller. To some extent, this correlation can be explained by the fact that galaxies with larger equivalent widths are more likely to be fainter; this is the case for the i_{775}-dropout sample (Figure 19, bottom panel). The correlation, however, seems to persist even when subsamples cut by absolute luminosities are considered, as illustrated in the top panel of Figure 19 where the size of the symbols scale with apparent z_{850} magnitude. In this latter case, only sources with spectroscopically detected detected and $z < 5.6$ have been considered (at $z > 5.6$, Lyα enters the z_{850} band). One potential physical explanation of this size behavior could lie in the masses of the objects. Lyα-emitting LBGs at $z \sim 3$–4 are found to have smaller stellar masses than objects lacking this emission (e.g., Gawiser et al. 2006). Pentericci et al. (2007) also found for the B_{435}-band dropout sample in the present work an average stellar mass of $(5 \pm 1) \times 10^9$ $M_\odot$ and $(2.3 \pm 0.8) \times 10^{10}$ $M_\odot$ for the emitters and absorbers, respectively. This further suggests that emitters may be associated with less massive dark matter halos and hence have

experienced a different star formation history compared to the absorption line galaxies. At higher redshift, this analysis is more critical because high-quality near-IR images (e.g., NICMOS) and deep spectroscopy are needed to identify the absorbers. Dow-Hygelund et al. (2007) found that Lyα-emitting i_{775}-band dropouts seem to be morphologically distinct from the general i_{775}-band dropout LBGs. We only report here that, on average, the h.l.r. for our sample of i_{775}-dropouts emitters is consistent with other observations (e.g., Stanway et al. 2004a, 2004b; Dow-Hygelund et al. 2007), with h.l.r. $\sim$ 0.″13 (Figure 19, lower panel). The only i_{775}-band dropout with QF = B without Lyα in emission (GDS J033233.19−273949.1) has h.l.r. = 0.″20. High-quality and deeper near-IR images and spectroscopy are necessary to investigate this issue.

9. CONCLUSIONS

In the present work, we have addressed the spectroscopic properties of LBGs at high redshift, selected from the GOODS Survey. We have discussed the efficiency of the photometric selection criteria adopted. We have extracted preliminary information from the spectral features and UV luminosity and compared it with analogous studies at lower redshift. Summarizing,

1. 109 out of 202 targeted LBGs have been spectroscopically confirmed in the redshift range $3.1 < z < 6.6$, according to B_{435}-, V_{606}-, and i_{775}-band dropout selections. This relatively low confirmation rate is largely due to the following two reasons: (1) the target list includes a relatively large fraction of faint sources, with 65 out of 202 or 32.2% of the sample having $z_{850} > 26$; and (2) the difficulty in determining redshifts for galaxies at $z < 3.6$ given our instrumental setup. Considering sources with determined redshifts, 96%, 89%, and 82% of the observed B_{435}-, V_{606}-, and i_{775}-band dropout samples have been confirmed in the expected redshift range, respectively. Twelve low-redshift interlopers have also been confirmed, 10 stars and two galaxies at $z < 2$. Five high-redshift galaxies have been serendipitously discovered, yielding a total of 114 redshifts measured beyond redshift 3.1 (38 of these with QF = C).
2. From the composite spectra of the three flavors of dropout (B_{435}-, V_{606}-, and i_{775}-band dropouts), we detect the typical spectral features of star-forming galaxies, namely a flat spectrum redward of Lyα, IGM attenuation and the Lyman limit blueward of Lyα, UV absorption lines (both high and low ionization), and Lyα seen in both emission or absorption. In particular, at $z \sim 4$, a comparison between the composite spectra of emitters and absorbers shows steeper spectral slopes and weaker UV absorption features for the emitters.
3. Galactic outflows have been identified at $z \sim 4$ by measuring the velocity offset between interstellar, Lyα, and nebular lines. The measured $\langle V_{\mathrm{Ly}\alpha} - V_{\mathrm{ISL}} \rangle = 370^{+270}_{-116}$ km s^{-1} is consistent with results at $z \sim 3$ by Shapley et al. (2003), considering the portion of their sample with similar Lyα equivalent widths to our sample. We derive $\langle V_{\mathrm{ISL}} - V_{\mathrm{nebular}} \rangle$ of -165 km s^{-1}, similar to the -150 km s^{-1} derived by Adelberger et al. (2003) at lower ($z \sim 3$) redshift. A similar offset (but less accurate because it is derived from the composite spectrum) has been detected in the V_{606}-dropout sample (redshift ~ 5), i.e., $\langle V_{\mathrm{Ly}\alpha} - V_{\mathrm{ISL}} \rangle \sim 500$ km s^{-1}. This supports the interpretation that outflows similar to those taking place at $z \sim 2$ and 3 are also observed in our samples of LBGs at $z \sim 4$ and 5.
4. The presence of a weaker Lyα equivalent width for dropouts with brighter UV luminosities ($M_{145} < -21$) is clear in the current spectroscopic sample (considering all categories). This trend has been recently noted by several authors, and may be naturally explained by a different evolution of bright UV LBGs with respect to the fainter ones. The brighter galaxies should be dustier and more evolved (and probably more massive) than the fainter ones, which show a larger spread of Lyα equivalent widths possibly due to assorted star formation histories.
5. The sample at $z \sim 4$ exhibits correlations between certain basic UV rest-frame morphological properties and spectroscopic properties such as the presence and strength of Lyα emission. In particular, emitters appear more compact and nucleated than absorbers. Law et al. (2007) find a similar "nucleation effect" at $z \sim 2$ and 3 in their BM/BX and LBG samples, and interpret this as a consequence of more dust in the absorbers leading to redder colors and more diffuse morphologies. Pentericci et al. (2009) analyze the photometric properties of the same sample as discussed here, and find that emitters are less massive and less dusty than absorbers. Focusing on the emitters, increasing Lyα equivalent widths correspond to decreasing stellar masses and extinction. The emitters, especially those with a large Lyα equivalent width, could be systems forming a relatively large fraction of their stellar mass during an intense burst of star formation. These putative proto-spheroids observed at $z \sim 4$ could include in significant numbers the progenitors of the compact massive early-type galaxies identified at $z \sim 2$ (e.g., Cimatti et al. 2008; van Dokkum et al. 2008; Buitrago et al. 2008). Such an evolutionary link is generally consistent with the observed spatial clustering properties and the stellar populations of LBGs at $z \sim 3$ and $\sim$4 (Giavalisco et al. 1998; Giavalisco & Dickinson 2001; Lee et al. 2006, 2008; Ouchi et al. 2005) and those of the BzK and DRG galaxies at $z \sim$ 2–2.5 (Kong et al. 2006; Quadri et al. 2008). The strength of spatial clustering increases with the mass of the galaxies and with redshift, as a consequence of gravitational evolution of structure. The observed larger spatial correlation length and larger stellar mass of the UV/optical-selected galaxies at $z \sim 2$ (Daddi et al. 2007; van Dokkum et al. 2006) are in overall quantitative agreement with the expected dependence of clustering with both mass and time, when compared to the less strongly clustered and less massive (in stellar content) UV-only selected galaxies at $z \sim 3$ and $\sim$4 (Adelberger et al. 2005). This suggests that the same populations of dark matter halos are being observed at different evolutionary stages of the growth of their galaxy hosts and spatial clustering.

We are grateful to the ESO staff in Paranal and Garching who greatly helped in the development of this programme. We acknowledge financial contribution from contract ASI/COFIN I/016/07/0 and PRIN INAF 2007 "A Deep VLT and LBT view of the Early Universe." E.V. thanks STScI and NOAO for hospitality during a visit in which this paper was conceived and partially written. E.V. thanks F. Calura for useful discussions about the dust properties of high-redshift galaxies. The work of D.S. was carried out at Jet Propulsion Laboratory, California Institute of Technology, under a contract with NASA.

REFERENCES

Abraham, R. G., van den Bergh, S., & Nair, P. 2003, ApJ, 588, 218
Adelberger, K. L., Steidel, C. C., Shapley, A. E., & Pettini, M. 2003, ApJ, 584, 45
Adelberger, K. L., et al. 1998, ApJ, 505, 18A
Adelberger, K. L., et al. 2005, ApJ, 619, 697
Ando, M., Ohta, K., Iwata, I., Akiyama, M., Aoki, K., & Tamura, N. 2007, PASJ, 59, 717
Ando, M., et al. 2006, ApJ, 645, 9
Bertin, E., & Arnouts, S. 1996, A&A, 117, 393
Bouwens, R. J., Illingworth, G. D., Blakeslee, J. P., & Franx, M. 2006, ApJ, 653, 53
Bouwens, R. J., Illingworth, G. D., Franx, M., & Ford, H. 2007, ApJ, 670, 928
Bruzual, G., & Charlot, S. 2003, MNRAS, 344, 1000
Buitrago, F., Trujillo, I., Conselice, C. J., Bouwens, R. J., Dickinson, M., & Yan, H. 2008, ApJL, submitted (arXiv:0807.4141)
Bunker, A. J., Stanway, E. R., Ellis, R. S., & McMahon, R. G. 2004, A&AS, 204, 9103
Bunker, A. J., et al. 2003, MNRAS, 342L, 47
Calzetti, D., Armus, L., Bohlin, R. C., & Kinney, A. L. 2000, ApJ, 533, 682
Cimatti, A., et al. 2008, A&A, 482, 21
Daddi, E., Cimatti, A., Renzini, A., Fontana, A., Mignoli, M., Pozzetti, L., Tozzi, P., & Zamorani, G. 2004, ApJ, 617, 746
Daddi, E., et al. 2007, ApJ, 670, 173
Dickinson, M., Papovich, C., Ferguson, H. C., & Budavári, T. 2003a, ApJ, 587, 25
Dickinson, et al. 2003b, in Mass of Galaxies at Low and High Redshift, ed. R. Bender & A. Renzini (New York: Springer), 324
Dickinson, M., et al. 2004, ApJ, 600, 99
Dow-Hygelund, C. C., et al. 2007, ApJ, 660, 47
Ferguson, H. C., et al. 2004, ApJ, 600, 107
Ford, H. C., et al. 1998, Proc. SPIE, 3356, 234
Frye, B., Broadhurst, T., & Benítez, N. 2002, ApJ, 568, 558
Gawiser, E., et al. 2006, ApJ, 642, L13
Giavalisco, M. 2002, ARA&A, 40, 579
Giavalisco, M., & Dickinson, M. 2001, ApJ, 550, 177
Giavalisco, M., Steidel, C. C., & Macchetto, F. D. 1996, ApJ, 470, 189
Giavalisco, M., et al. 1998, ApJ, 503, 543
Giavalisco, M., et al. 2004a, ApJ, 600, L93
Giavalisco, M., et al. 2004b, ApJ, 600, 103
Grazian, A., et al. 2006, A&A, 449, 951
Guhathakurta, P., Tyson, J. A., & Majewski, S. R. 1990, ApJ, 357, L9
Hamana, T., Yamada, T., Ouchi, M., Iwata, I., & Kodama, T. 2006, MNRAS, 369, 1929
Iwata, I., Ohta, K., Tamura, N., Ando, M., Wada, S., Watanabe, C., Akiyama, M., & Aoki, K. 2003, PASJ, 55, 415
Kong, X., et al. 2006, ApJ, 638, 72
Law, D. R., et al. 2007, ApJ, 656, 1
Lee, K.-S., Giavalisco, M., Conroy, C., Wechsler, R. H., Ferguson, H. C., Somerville, R. S., Dickinson, M. E., & Urry, C. M. 2008, ApJ, submitted (arXiv:0808.1727)
Lee, K.-S., Giavalisco, M., Gnedin, O. Y., Somerville, R. S., Ferguson, H. C., Dickinson, M., & Ouchi, M. 2006, ApJ, 642, 63
Leitherer, L., et al. 1999, ApJS, 123, 3
Lisker, T. 2008, ApJS, 179, 319
Lotz, J. M., Madau, P., Giavalisco, M., Primack, J., & Ferguson, H. C. 2006, ApJ, 636, 592L
Madau, P. 1995, ApJ, 441, 18
Madau, P., Pozzetti, L., & Dickinson, M. 1998, ApJ, 498, 106
Maiolino, R., et al. 2008, A&A, 488, 463M
Malhotra, S., et al. 2005, ApJ, 626, 666
Mori, M., & Umemura, M. 2006, Nature, 440, 644
Oke, J. B. 1974, ApJS, 27, 21
Ouchi, M., et al. 2005, ApJ, 635, 117
Overzier, R. A., Heckman, T. M., Kauffmann, G., Seibert, M., & Rich, R. M. 2008, ApJ, 677, 37
Papovich, C., Dickinson, M., & Ferguson, H. C. 2001, ApJ, 559, 620
Papovich, C., Giavalisco, M., Dickinson, M., Conselice, C. J., & Ferguson, H. C. 2003, ApJ, 598, 827
Pentericci, L., Grazian, G., Fontana, A., Castellano, M., Giallongo, E., Salimbeni, S., & Santini, P. 2009, A&A, 494, 553
Pentericci, L., Grazian, A., Fontana, A., Salimbeni, S., Santini, P., de Santis, C., Gallozzi, S., & Giallongo, E. 2007, A&A, 471, 433
Pettini, M., Steidel, C. C., Adelberger, K. L., Dickinson, M., & Giavalisco, M. 2000, ApJ, 528, 96
Popesso, P., et al. 2009, A&A, 494, 443
Quadri, R. F., et al. 2008, ApJ, 685, 1
Ravindranath, S., et al. 2006, ApJ, 652, 963
Reddy, N. A., et al. 2008, ApJS, 175, 48
Renzini, et al. 2003, The Mass of Galaxies at Low and High Redshift, ed. R. Bender & A. Renzini (New York: Springer), 332
Riess, A. G., Li, W., Stetson, P. B., & Filippenko, A. V. 2005, ApJ, 627, 579
Riess, A. G., et al. 2004, ApJ, 607, 665
Schaerer, D., & Verhamme, A. 2008, A&A, 480, 369
Shapley, A. E., Steidel, C. C., Adelberger, K. L., Dickinson, M., & Giavalisco, P. M. 2001, ApJ, 562, 95
Shapley, A. E., Steidel, C. C., Pettini, M., & Adelberger, K. L. 2003, ApJ, 588, 65
Shapley, A. E., et al. 2005, ApJ, 626, 698
Shimasaku, K., Ouchi, M., Furusawa, H., Yoshida, M., Kashikawa, N., & Okamura, S. 2005, PASJ, 57, 447
Songaila, A. 2004, AJ, 127, 2598
Spinrad, H., Stern, D., Bunker, A., Dey, A., & Lanzetta, K. 1998, AJ, 116, 2617
Stanway, E. R., Bunker, A. J., & McMahon, R. G. 2003, MNRAS, 342, 439
Stanway, E. R., Bunker, A. J., McMahon, R. G., Ellis, R. S., Treu, T., & McCarthy, P. J. 2004a, ApJ, 607, 704
Stanway, E. R., et al. 2004b, ApJ, 604, L13
Steidel, C. C., Adelberger, K. L., Giavalisco, M., Dickinson, M., & Pettini, M. 1999, ApJ, 519, 1
Steidel, C. C., Adelberger, K. L., Shapley, A. E., Pettini, M., Dickinson, M., & Giavalisco, M. 2003, ApJ, 592, 728
Steidel, C. C., Giavalisco, M., Dickinson, M., & Adelberger, K. L. 1996a, AJ, 112, 352
Steidel, C. C., Giavalisco, M., Pettini, M., Dickinson, M., & Adelberger, K. L. 1996b, ApJ, 462, 17
Stern, D., Bunker, A., Spinrad, H., & Dey, A. 2000, ApJ, 537, 73S
Taniguchi, Y., et al. 2005, PASJ, 57, 165
Tapken, C., Appenzeller, I., Noll, S., Richling, S., Heidt, J., Meinkohn, E., & Mehlert, D. 2007, A&A, 467, 63
Thompson, R. I., et al. 2006, ApJ, 647, 787
van Dokkum, P. G., Quadri, R., Marchesini, D., & Rudnick, G. 2006, ApJ, 638, 59
van Dokkum, P. G., et al. 2003, ApJ, 611, 703
van Dokkum, P. G., et al. 2008, ApJ, 677, 5
Vanzella, E., et al. 2005, A&A, 434, 53
Vanzella, E., et al. 2006, A&A, 454, 423
Vanzella, E., et al. 2008, A&A, 478, 83
Verhamme, A., Schaerery, D., Atek, A., & Tapken, C. 2008, A&A, 491, 89
Verhamme, A., Schaerer, D., & Maselli, A. 2006, A&A, 460, 397
Wiklind, T., Dickinson, M., Ferguson, H. C., Giavalisco, M., Mobasher, B., Grogin, N. A., & Panagia, N. 2008, ApJ, 676, 781
Yan, H., Dickinson, M., Giavalisco, M., Stern, D., Eisenhardt, P. R. M., & Ferguson, H. C. 2006, ApJ, 651, 24
Yoshida, M., et al. 2006, ApJ, 653, 988